4.1 X-Ray Diffraction Investigation

X-ray diffraction (XRD) is essential to illustrate the effect of addition of ethylene carbonate (EC) on the degree of crystalinity of the solid acid in the polymer matrix. Fig.(4.1) shows XRD pattern for ((PVA: 0.5 $NaHSO_4$) / x EC) where x = 0, 9.9, 13.2 and 16.5 wt.%. A peak at 2θ=23.54° was observed in Fig (4.1a), the observed peak matched quite well with JCPDS file No.85-2043 for $NaHSO_4$. There is a relative decrease in the intensity of this peak with addition of EC. This may be due to the increase of amorphous nature of polymer electrolyte with the addition of EC. Hodge et al [66] established a correlation between the intensity of the peak and the degree of crystallinity. They observed that the intensity of XRD pattern decreases as the amorphous nature increases with the addition of plasticizer.

The structure investigation using XRD has been extended to show the influence of Si on plasticized solid acid polymer electrolyte (PSAPE). Fig.(4.2) shows XRD pattern for ((PVA: 0.5 $NaHSO_4$) : 9.9 wt.% EC/ y Si) where y = 0, 0.15, 0.75, 1.2 and 3.75 wt.%. There was a noticeable change in XRD peaks for samples mixed with Si in addition to the appearance of additional peaks. The results indicated that converged broad hump when the amount of Si content to (PSAPE) and appear another two peaks at 2θ=13.6°, 2θ=16.6°. The observed peak matched quite well with JCPDS file No.490076 for silicon oxide sulfur (SiOS). The results suggest the occurrence of a significant new structure with the polymer electrolyte. The formation of such structure suggests that the addition of Si on the matrix cause an electrostatic interaction between Si and SO_4^{--}. This in turn leads to move ionization of SAPE ($NaHSO_4$) to form more mobile H^+ and Na^+.

The average particle size of SAPE can be calculated using the first sphere approximation of Debye–Scherrer formula [67],

$$D = \frac{0.9\lambda}{B\cos\theta} \qquad (4.1)$$

where D is the average diameter of the crystals, λ is the wavelength of X-ray radiation, B is the full width at half maximum intensity of the peak and θ is the incident angle.The average particle size of $NaHSO_4$ is equal to~ 41nm. The average size of nanopartiacle SiOS is equal to ~ 11nm, where the size of SiOS in polymer matrix obtained at different mentioned Si ratio are shown in Table (4.1).

Table (4.1): Extracted values of the average particle size of nanocomposite for ((PVA: 0.5 $NaHSO_4$) : 9.9wt. % EC/ y Si) with y = 0.15, 0.75, 1.2 and 3.75 wt. %.

y wt.% Si	Particle size (nm)
0.15	**11.1**
0.75	**11.5**
1.2	**11.7**
3.75	**11.4**

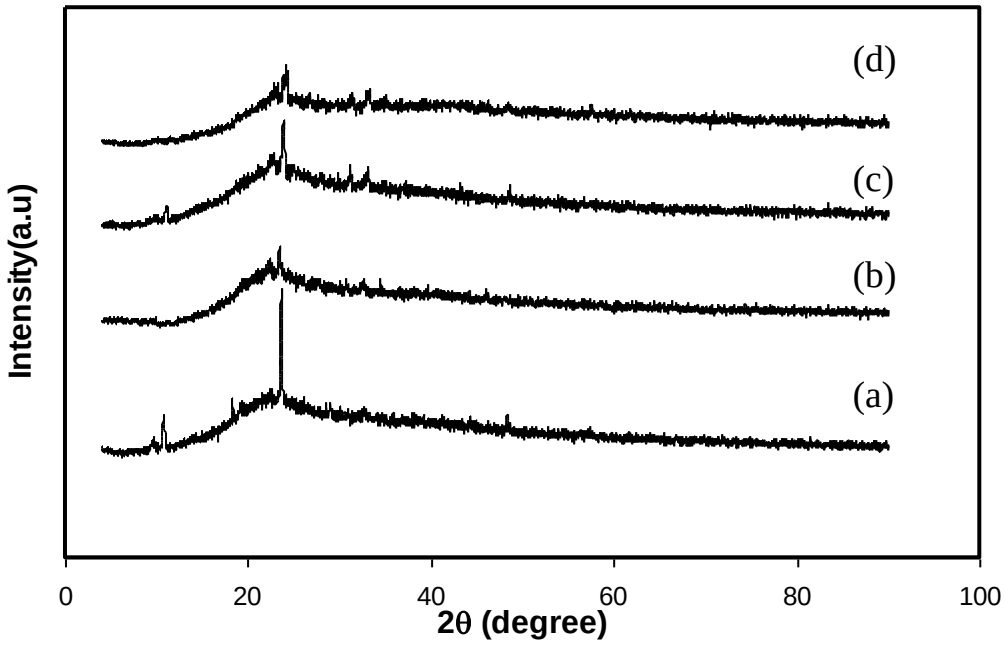

Fig.(4.1): XRD pattern for ((PVA: 0.5 $NaHSO_4$) / x EC), (a) x=0, (b) x=9.9, (c) x=13.2 & (d) x=16.5 wt.%.

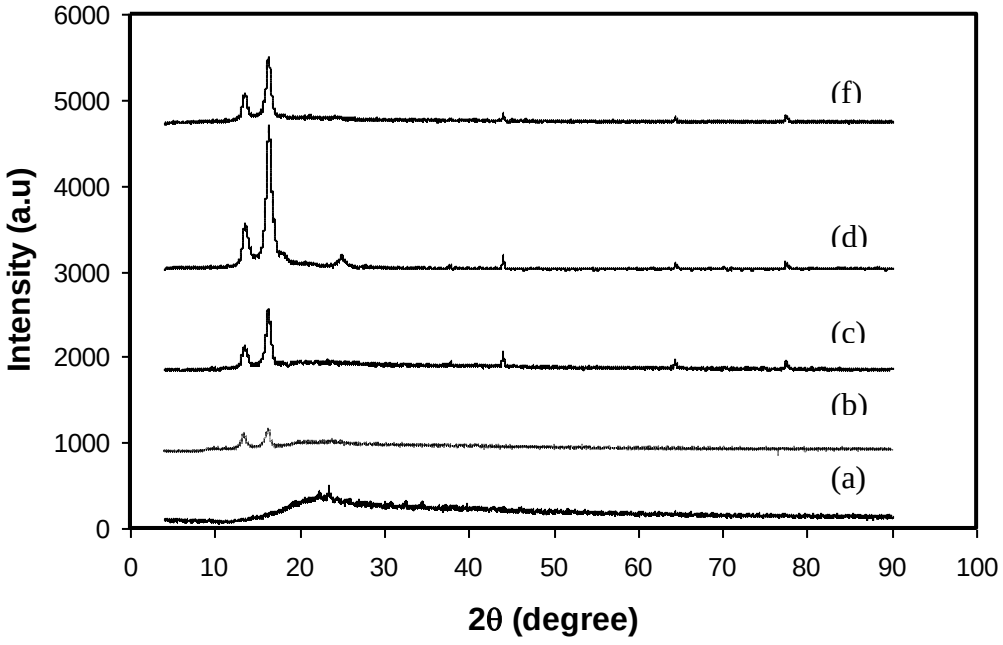

Fig.(4.2): XRD pattern for ((PVA: 0.5 $NaHSO_4$) : 9.9 wt.% EC/ y Si), (a) y=0, (b) y=0.15, (c) y=0.75, (d) y=1.2 & (f) y=3.75 wt.%.

4.2 Scanning Electron Microscope Investigation

In the present section scanning electron microscopy investigation has been used to show the infulence of (EC) on polymer electrolyte surface morpholgy which has effect on the other physical prameters. Fig. (4.3, a-c) shows scanning electron micrograph of ((PVA: 0.5 $NaHSO_4$) / x EC) with x = 0, 9.9, and 13.2 wt.%. A comparison of the surface morphology shows marked change in the surface morphology and texture of the polymer electrolytes by the addition of EC. Surface roughening and crystalline texture of internal morphology appear to change gradually by addition of EC concentration. These effects ultimately result in the appearance of a smooth texture of the surface. Such changes can be attributed to the fact that plasticization causes a reduction in the crystallinity of the host polymer (i.e., poly vinyl alcohol) and subsequent enhancement in the overall amorphous fraction in the material. This observation appears to be in good agreement with the XRD results.

Fig. (4.4, a-d) shows scanning electron micrograph of ((PVA: 0.5 $NaHSO_4$): 9.9 wt. % EC/ y Si) with y = 0.15, 0.75, 1.2 and 3.75 wt. %. In case of Si there are long single crystals like particles having rod-shaped morphology. The sample morphology surface was uniform but with roughness where an increase in the degree of roughness with increasing Si concentration indicates the formation of new structure in the host matrix in agreement with XRD. The difference in morphology with the presence of Si in electrolyte is consistent with the significant differences in the ionic conductivity of these electrolytes.

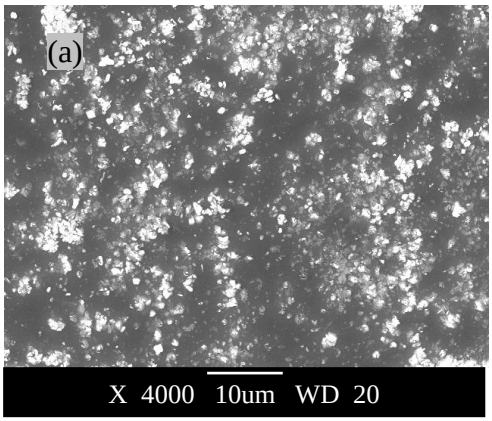

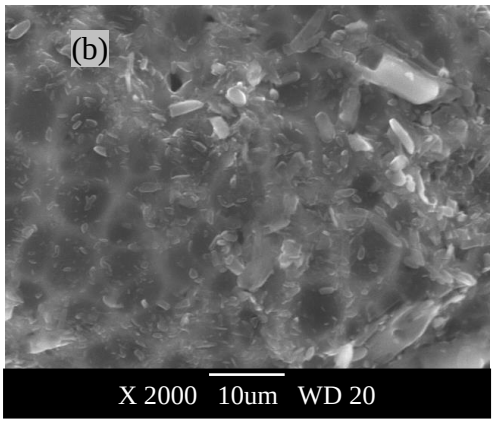

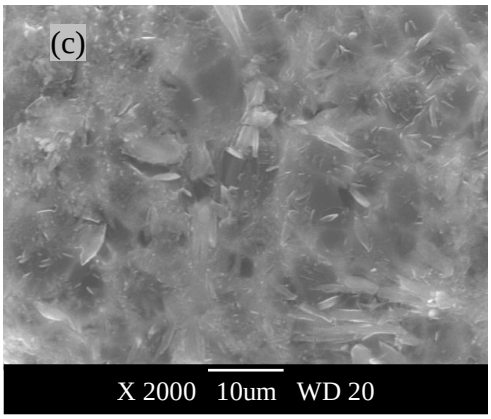

Fig.(4.3): SEM microscope for ((PVA: 0.5 $NaHSO_4$) / x EC),where (a) x=0, (b) x=9.9 & (c) x=13.2 wt.%.

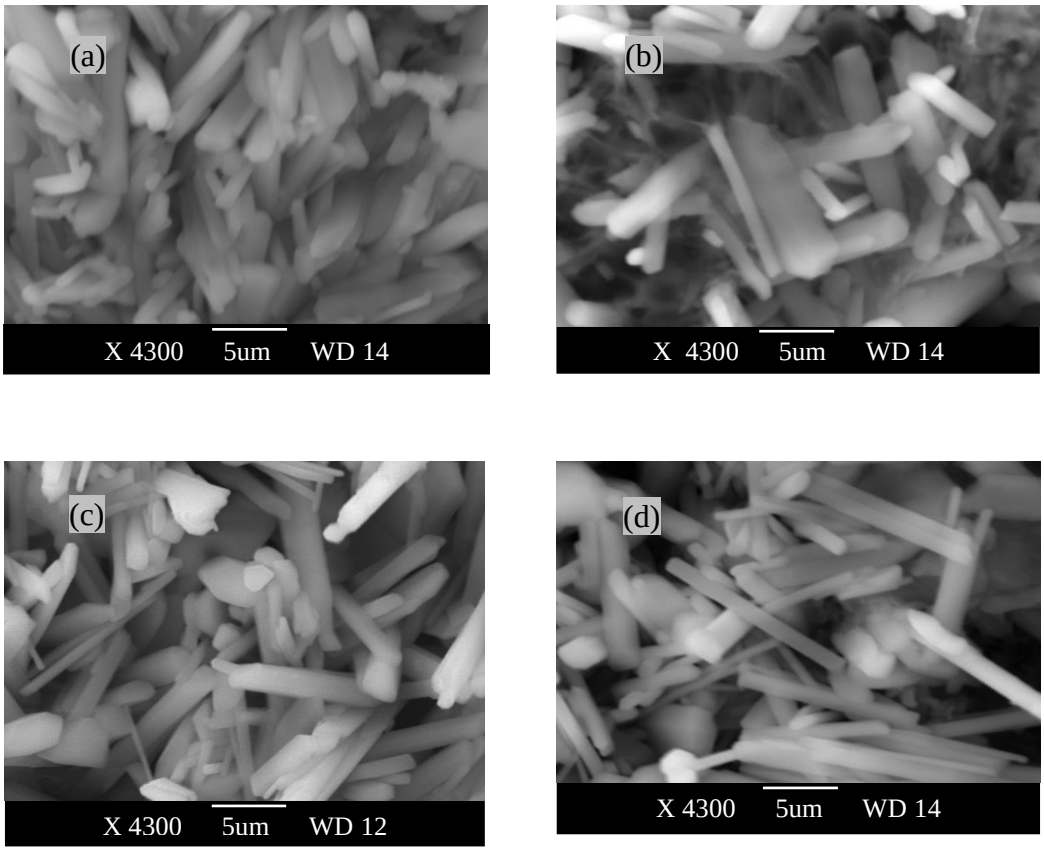

Fig.(4.4): SEM for ((PVA: 0.5 $NaHSO_4$) : 9.9 wt.% EC/ y Si), where (a) y=0.15, (b) y=0.75, (c) y=1.2 & (d) y=3.75 wt.%.

4.3 Thermogravimetric Analysis

Thermogravometric analysis (TGA) is considered as the most important method for studying thermal stability of polymer electrolytes. This is an important property for polymer electrolytes during application in energy conversion cells. Fig.(4.5) shows the TGA curves of the ((PVA: 0.5 $NaHSO_4$) / x EC) where x=0, 9.9, 13.2 and 16.5 wt. %. The general behavior shows two main degradation stages. It is evident that initial weight loss up to 100 °C is closely associated with the loss of absorbed water molecules (dehydration). The second weight loss occurs between 156 and 166°C for all samples with maximum weight loss rate at certain temperatures. The first deravative of weight loss against temperture has been used to determine the maximum weight loss which indicate the effective temperture of deggradation. In addition the first TGA onset temperature was corresponding to water dehydration while the second onset temperature in the range 156 to 166 °C corresponds to polymer decomposition, and those two onset temperatures were calculated and summarized in Table (4.2).

Fig.(4.6) shows the TGA curves of the ((PVA: 0.5 $NaHSO_4$) : 9.9 wt.% EC/ y Si) where y = 0.15, 0.75, 1.2 and 3.75 wt.%. The results suggest that the introduction of Si into the PVA chains decrease the thermal stability of the given polymer electrolyte

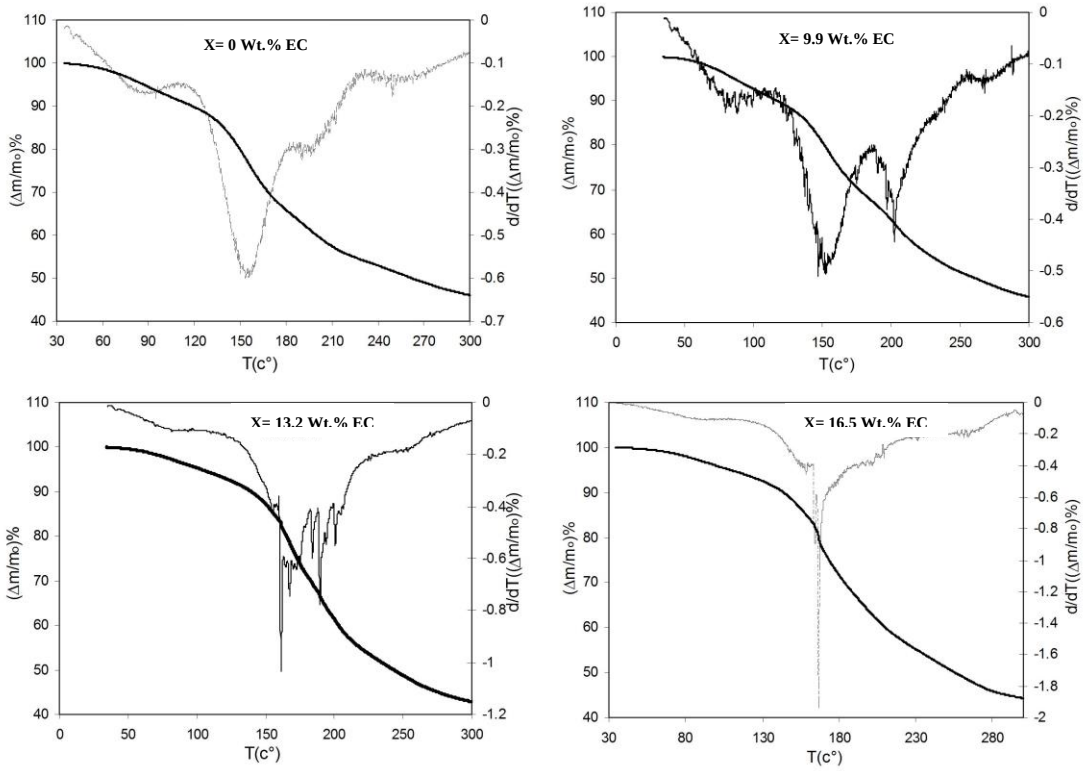

Fig.(4.5): TGA thermograms (weight loss fraction) versus temperature for ((PVA: 0.5 $NaHSO_4$) / x wt.% EC).

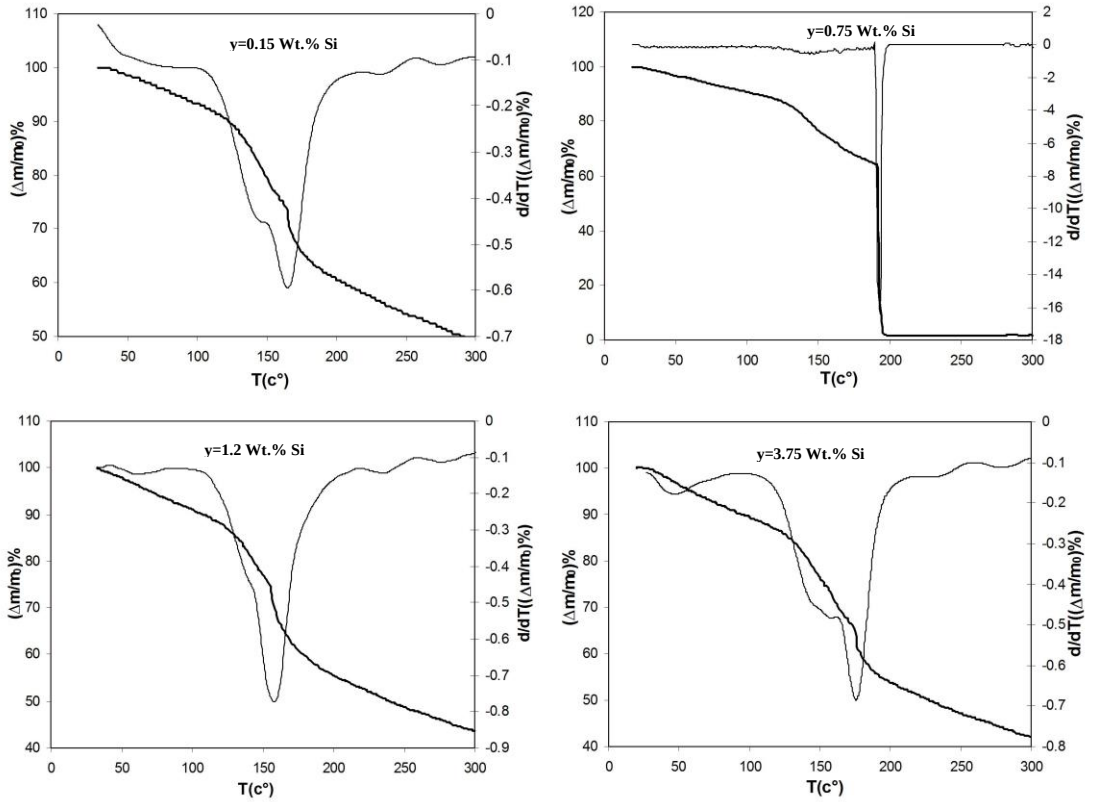

Fig.(4.6): TGA thermograms (weight loss fraction) versus temperature for ((PVA: 0.5 $NaHSO_4$) : 9.9 wt.% EC/ y Si).

The activation energy for the thermal decomposition of the samples can be calculated using the integral equation of Coates and Redfern[68].

$$\log[\frac{-\log(1-\alpha)}{T^2}] = \log[\frac{(1-2RT/E)AR}{\beta E}] - \frac{E_a}{2.303RT} \quad (n=1) \qquad (4.2)$$

Where T is the absolute temperature, E_a is the activation energy (J mol^{-1}), R is the universal gas constant (8.13 J mol^{-1} K^{-1}), and n is the order of reaction β is the heating rate and the fractional conversion, α, for weight loss is given by,

$$\alpha = \frac{w_i - w_t}{w_i - w_f}$$

Where w_i is the initial weight, w_t is the weight at given temperature and w_f is the final weight of the sample, respectively. By plotting $\log[-\log(1-\alpha)/T^2]$ against $1000/T$ for each sample Fig. (4.7) and Fig. (4.8), straight lines are obtained. Then, the apparent activation energies for the decomposition E_{a1} for ((PVA: 0.5 $NaHSO_4$) / x EC) and the activation energy E_{a2} for ((PVA: 0.5 $NaHSO_4$): 9.9 wt. % EC/ y Si), are calculated and given in Tables (4.2) & (4.3), respectively.

It is noticed that, the optimum values for E_{a1} for x =9.9 wt. % EC. This confirms that the maximum thermal stability is for this concentration.

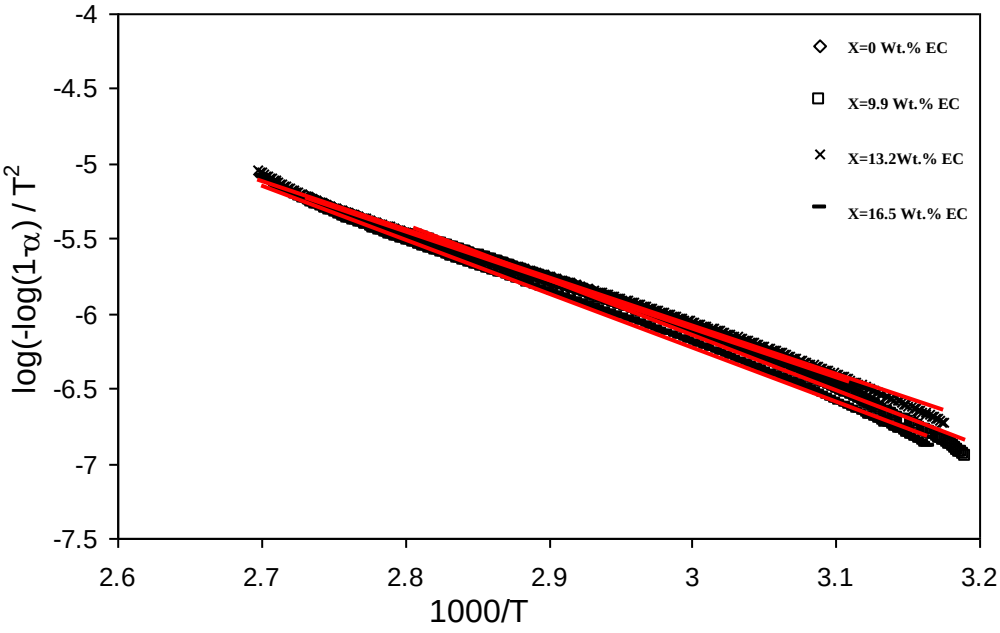

Fig.(4.7): The dependence of $\log[\frac{-\log(1-\alpha)}{T^2}]$ **on** $1000/T$ **for ((PVA:0.5 $NaHSO_4$)/ x EC).**

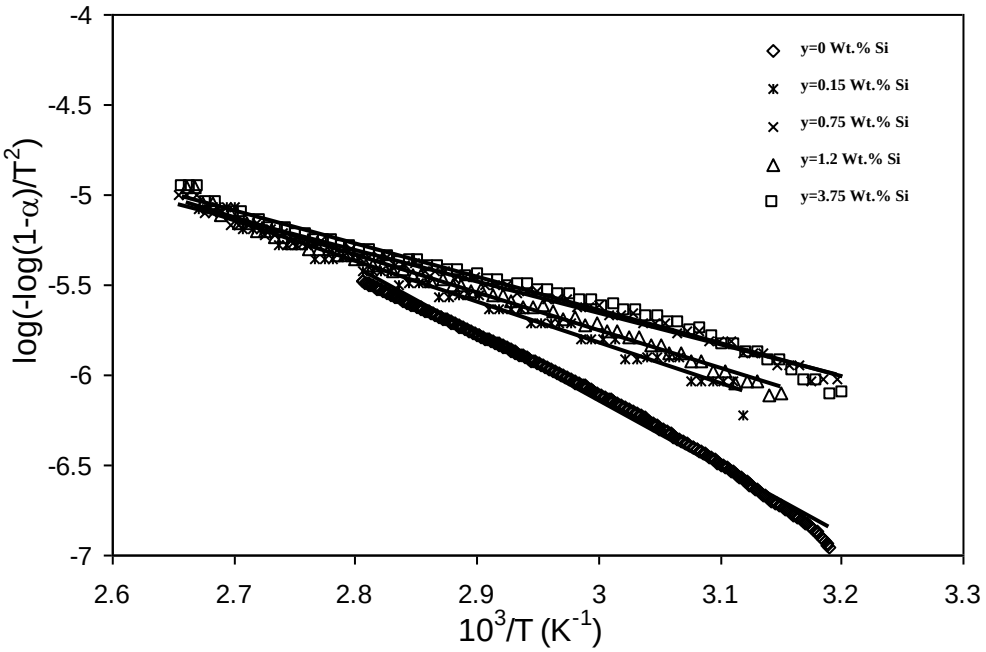

Fig.(4.8): The dependence of $\log[\frac{-\log(1-\alpha)}{T^2}]$ **on** $1000/T$ **for ((PVA:0.5 $NaHSO_4$): 9.9 wt. % EC/ y Si).**

Table (4.2): The values of the apparent activation energies, E_{a1} for ((PVA: 0.5 $NaHSO_4$): x EC) polymer electrolytes.

x wt.% EC	Activation energy (Ea_1) (eV)	$T_{onset(1)}$ (^{o}c)	$T_{onset(2)}$ (^{o}c)
0	0.64	85	156
9.9	0.72	82	165
13.2	0.64	83	153
16.5	0.71	85	166

Table (4.3): The values of the apparent activation energies, E_{a2} for ((PVA: 0.5 $NaHSO_4$): 9.9 wt. % EC/ y Si) polymer electrolytes.

y wt.% Si	Activation energy (E_{a2}) (eV)
0.15	0.43
0.75	0.38
1.2	0.43
3.75	0.40

4.4 FTIR Spectroscopy

FTIR is an authentic technique to deduce the possible interactions between the chemical constituents in polymer electrolytes. The FTIR spectrum exhibits several bands characteristic of stretching and bending vibrations of O–H, C–H, C=C and C–O bonds.

The FTIR spectrum of pure PVA are shown in Table (4.5) a broad and a strong band at 3538-3115 cm^{-1} is assigned to O–H stretching vibration of hydroxyl groups of PVA. A weak band is observed at 2163 cm^{-1}, which has been assigned to the combination frequency of (CH + CC). The bands at 1736 cm^{-1} corresponds to streching C=C bond. The strong band at 1100 cm^{-1} has been attributed to the stretching mode of C-O bond.

While in case of PVA with dopant, the evidence of complexation is observed through the change in intensity, shape, position and in the formation of new peaks. Fig.(4.9) shows FTIR spectra for ((PVA: 0.5 $NaHSO_4$) : x EC). FTIR spectra shows shift in some bands and change in the intensities of other bands comparing with pure PVA. This gives a clear indication of the specific interactions in the polymer matrix. The band observed at 2950 cm^{-1} indicates an asymmetry in stretching mode of CH_2 group in pure PVA and its slightly shifted in the complexed films. The characteristic vibrational band at 1100 cm^{-1} is assigned to C–O stretching of alcohols and is shifted in the complexed films respectively. C–C stretching occurring at 1246 cm^{-1} in pure PVA is shifted in the complexes films [10], see Table (4.4). The appearance of new peaks with the addition of EC or their disappearance in the FTIR spectra directly indicates the complexation of the polymer.

Fig. (4.10) shows the FTIR curves of the ((PVA: 0.5 $NaHSO_4$) : 9.9 wt.% EC/ y Si) where y =(0.15, 0.75, 1.2 and 3.75 wt.%) polymer electrolytes. The pure Si shows a characteristic band at 808cm^{-1}, Table (4.5) shows symmetric Si–O–Si band, asymmetric band Si–O–Si, and Si–OH band [71] for different Si concentration.

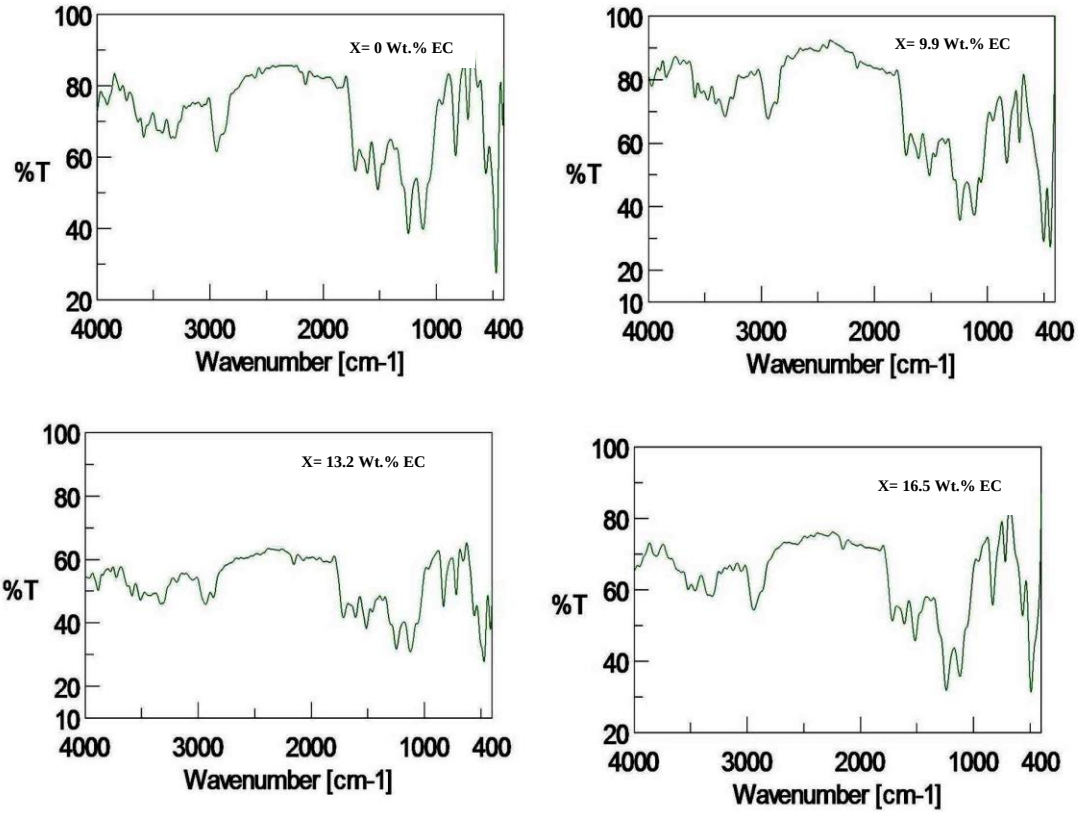

Fig.(4.9): FTIR spectra for ((PVA: 0.5 $NaHSO_4$) / x EC) where x= (0, 9.9, 13.2and 16.5 wt.%).

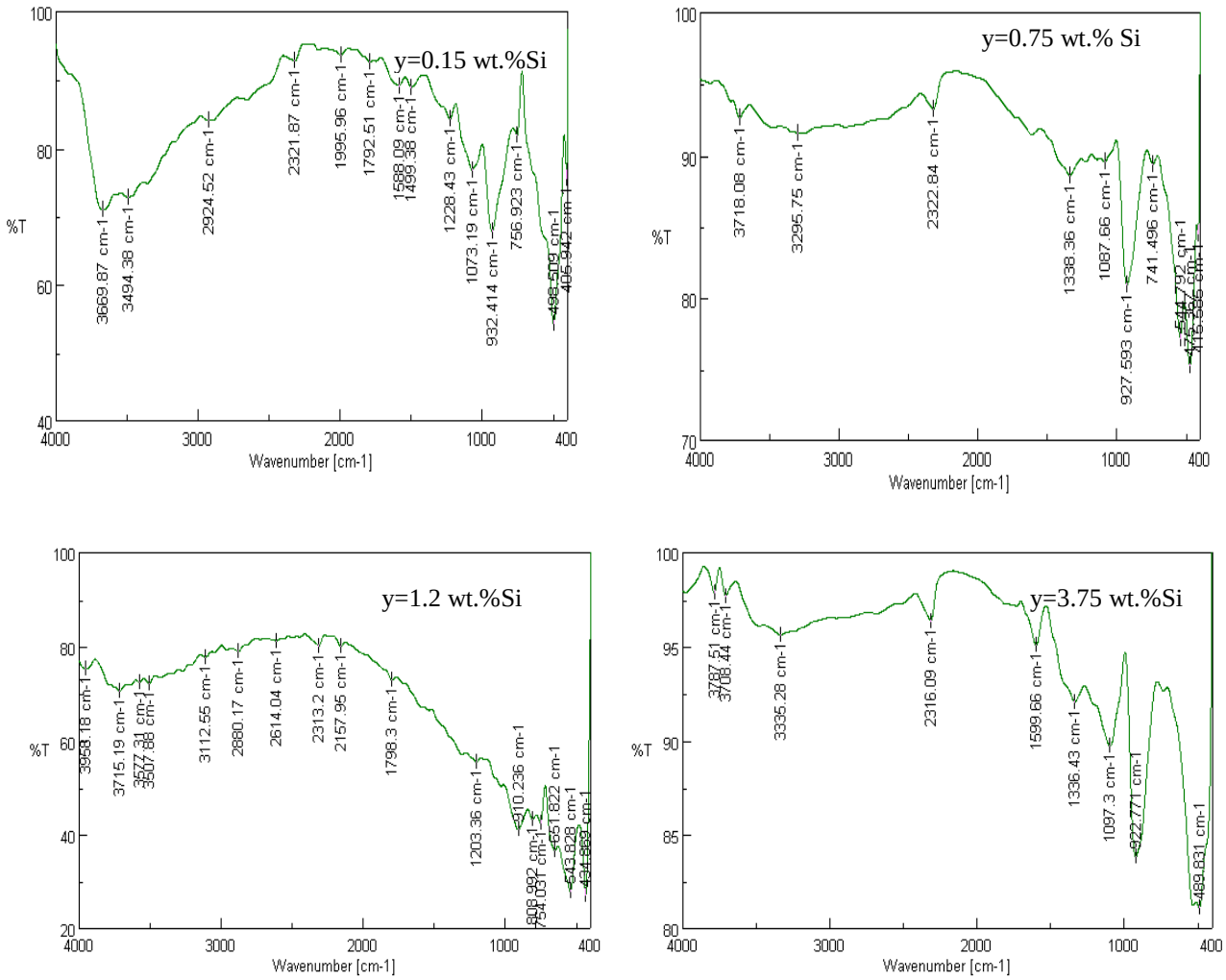

Fig.(4.10): FTIR spectra for ((PVA: 0.5 $NaHSO_4$) : 9.9 wt.% EC/ y Si).

Table (4.4): FTIR absorption bands positions and their assignments for pure PVA and ((PVA: 0.5 $NaHSO_4$) / x EC) with x= (0, 9.9, 13.2and 16.5 wt. %).

Vibration frequency (cm^{-1}) for pure PVA	Band assignment	Wt.%EC			
		x=0	x=9.9	x=13.2	X=16.5
3538-3115	O–H stretching	3422	3475	3510	3522
2950	CH_2 asymmetric stretching	2941	2940	2935	2943
2163	combination frequency of (CH + CC)	2165	2170	2169	2172
1246	C-C	1246	1244	1247	1240
1100	C-O	1116	1116	1124	1119

Table (4.5): FTIR Absorption bands positions and their assignments for ((PVA: 0.5 $NaHSO_4$): 9.9wt. % EC/ y Si) with y (0.15, 0.75, 1.2 and 3.75 wt. %).

Band assignment	wt.% Si			
	y= 0.15	y=0.75	y=1.2	y=3.75
symmetric Si–O–Si stretch	741	756	754	759
asymmetric Si–O–Si stretch	1087	1083	1089	1097
Si–OH stretch	927	932	910	922

4.5 Complex Impedance Analysis

The complex spectrum analysis of pure and plasticized SAPE has been carried out with an aim to observe the role of plasticizer in governing the electrical properties of ((PVA: 0.5 $NaHSO_4$) / x EC). Fig.(4.11) shows the complex impedance spectra of ((PVA: 0.5 $NaHSO_4$) / x EC) with x= (0, 3.3, 6.6, 9.9, 13.2, 16.5& 19.8 wt. %) at 303 K, 313 K. It is noticed that, semicircle does not pass through the origin, and the equivalent circuit consisting of the parallel resistance (bulk resistance, R_b) and the capacitance (bulk capacitance, C_b) network in series with contact resistance [72]. Symbols Z´ and Z´´ refer to the real and imaginary components, respectively. The bulk resistance was used subsequently for evaluation the bulk conductivity,

$$\sigma_b = \frac{t}{R_b A} \qquad (4.3)$$

Where R_b is the bulk resistance, t is the thickness of the sample and A is the cross sectional area of the sample.

Fig.(4.12) illustrates the variation of bulk conductivity with EC concentration at room temperature. It can be observed that the ionic conductivity values increases with increasing plasticizer content up to 9.9 wt. % EC and then it decreases. The variation in conductivity with EC concentrations may be explained in terms of the number of free mobile ions. In principle, $\sigma = nq\mu$ where n is the number of free mobile ions, q is the ionic charge and μ is ionic mobility. Assuming μ to be constant σ_b increases when n increases. At the first, the increase in conductivity could be attributed to the increase in the number of free mobile ions due to dissociation of ions up to 9.9 wt. % EC. The reduction in conductivity of

the electrolyte containing high amounts plasticizer (greater than 9.9 wt. % EC) could be attributed to the increase in ion pair's. Ions pairing that lead to the formation of aggregates form a more viscous medium which reduces the mobility of the charge carrier [73]. In this concentration range, the rate of ion association has to be greater than the rate of ion dissociation, and the distance between dissociated ions may become too close that are able to recombine and form neutral ion-pairs and do not contribute towards conductivity [74].

In polymer electrolytes, there are two possible mobile ionic species, i.e., cations and anions. The type of cation expected to be responsible for the ionic conductivity in ((PVA: 0.5 $NaHSO_4$) / x EC) system is H^+ ion. This H^+ ion can hop from one site to another leaving a vacancy which will be filled by another H^+ ion from a neighbouring site. Thus, the charge transport is carried out by structure diffusion or better known as Grotthus mechanism, i.e., the conduction occurs due to a dynamical effect of the anion HSO_4^- reorientation that reinforce the proton transfer in the complex[75].

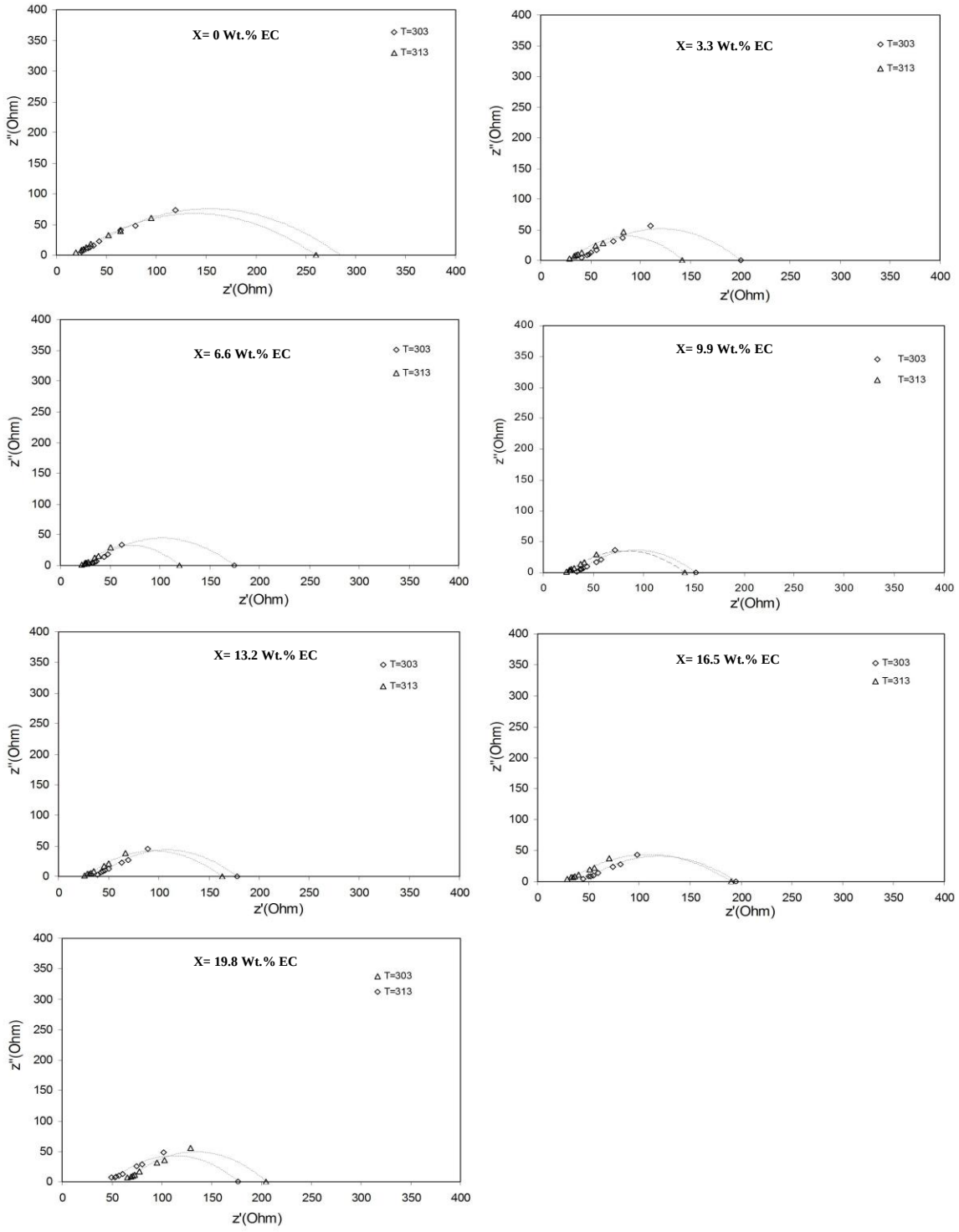

Fig.(4.11): Complex Cole– Cole plot of impedance for ((PVA: 0.5 $NaHSO_4$) / x EC) at T=303K, T=313K.

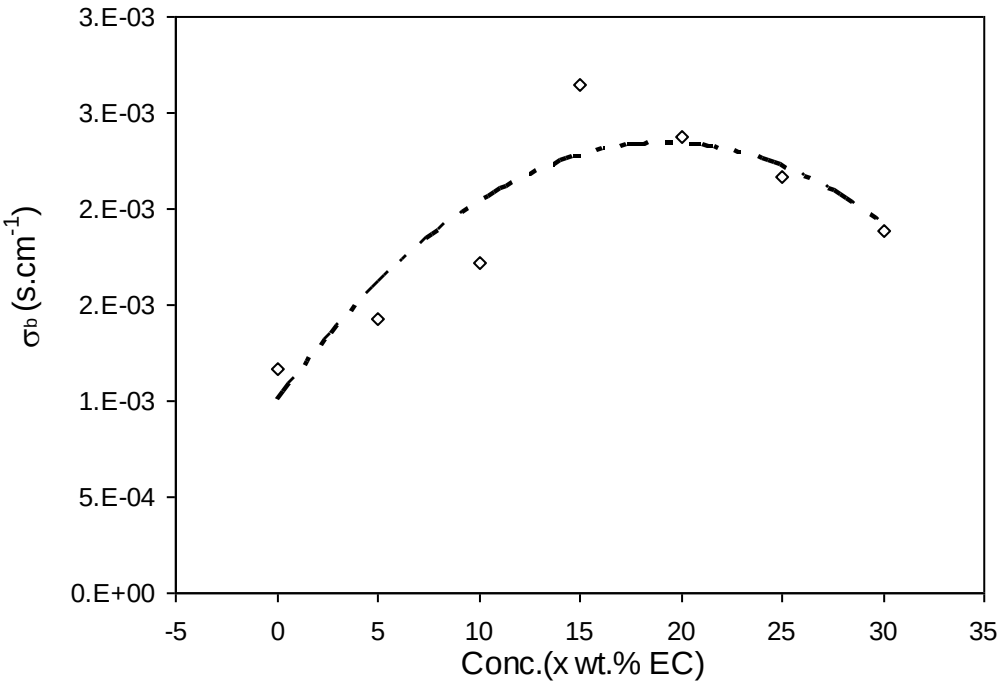

Fig.(4.12): Bulk conductivity of ((PVA: 0.5 $NaHSO_4$) / x EC) polymer electrolyte against EC concentration.

The values of σ_b have been obtained at different temperature. Fig.(4.13) shows the variation of the bulk conductivity σ_b for ((PVA: 0.5 $NaHSO_4$) / xwt. % EC) with temperature which obey Arrhenius relation [76],

$$\sigma_b T = (\sigma_o)\exp(-\frac{\Delta E_b}{KT}) \qquad (4.4)$$

where (σ_o) is temperature independent constant, ΔE_b is the bulk activation energy. The values of the activation energy ΔE_b are obtained using the least square fitting of equation (4.4) and listed in Table (4.6). It is noticed that ΔE_b decreases with increaseing EC concentration.

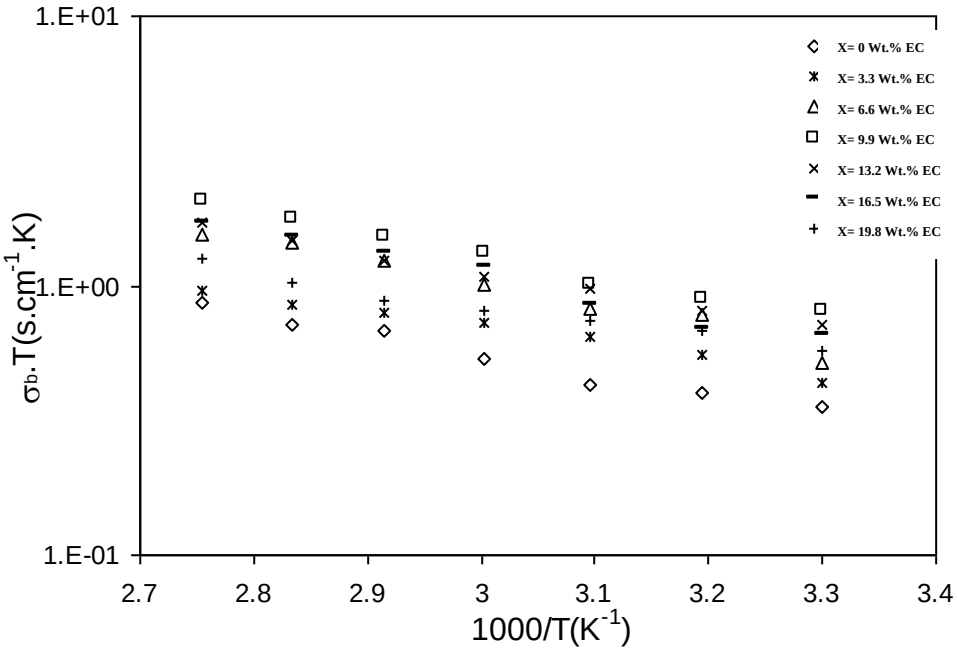

Fig.(4.13): Temperature dependence of bulk conductivity of ((PVA: 0.5 $NaHSO_4$) / x EC) at different concentrations of EC.

Table (4.6): Effect of EC concentration on the bulk activation energies (ΔE_b) of ((PVA: 0.5 $NaHSO_4$) / x EC) with different EC concentration.

x wt.% (EC)	ΔE_b(eV)
0	0.14
3.3	0.12
6.6	0.17
9.9	0.16
13.2	0.13
16.5	0.16
19.8	0.11

Fig.(4.14) shows the complex impedance spectra of ((PVA: 0.5 $NaHSO_4$) : 9.9 wt.% EC/ y Si) with y= (0.15, 0.75, 1.2& 3.75 wt.%) at temperatures 303 & 313 K. Impedance plot for all samples indicated that, semicircle does not pass through the origin. Its corresponding to the equivalent circuit consisting of parallel resistance (bulk resistance, R_b) and the capacitance (bulk capacitance, C_b) network in series with resistance (contact resistance)[72]. The bulk resistance was used subsequently for evaluation the bulk conductivity by equation (4.3).

Fig.(4.15) shows the variation of bulk conductivity for ((PVA: 0.5 $NaHSO_4$) : 9.9 wt.% EC/ y Si) with y= (0.15, 0.75, 1.2& 3.75 wt.%) at room temperature. It can be observed that the bulk conductivity value increase with increasing Si concentration. As the concentration of Si increases bulk conductivity increase. The addition of Si on the matrix cause in electrostatic interaction between Si and SO_4^{--}. This in turn leads to move ionization of SAPE ($NaHSO_4$) to form more mobile H^+. This causes an increase in the conductivity of the samples containing Si.

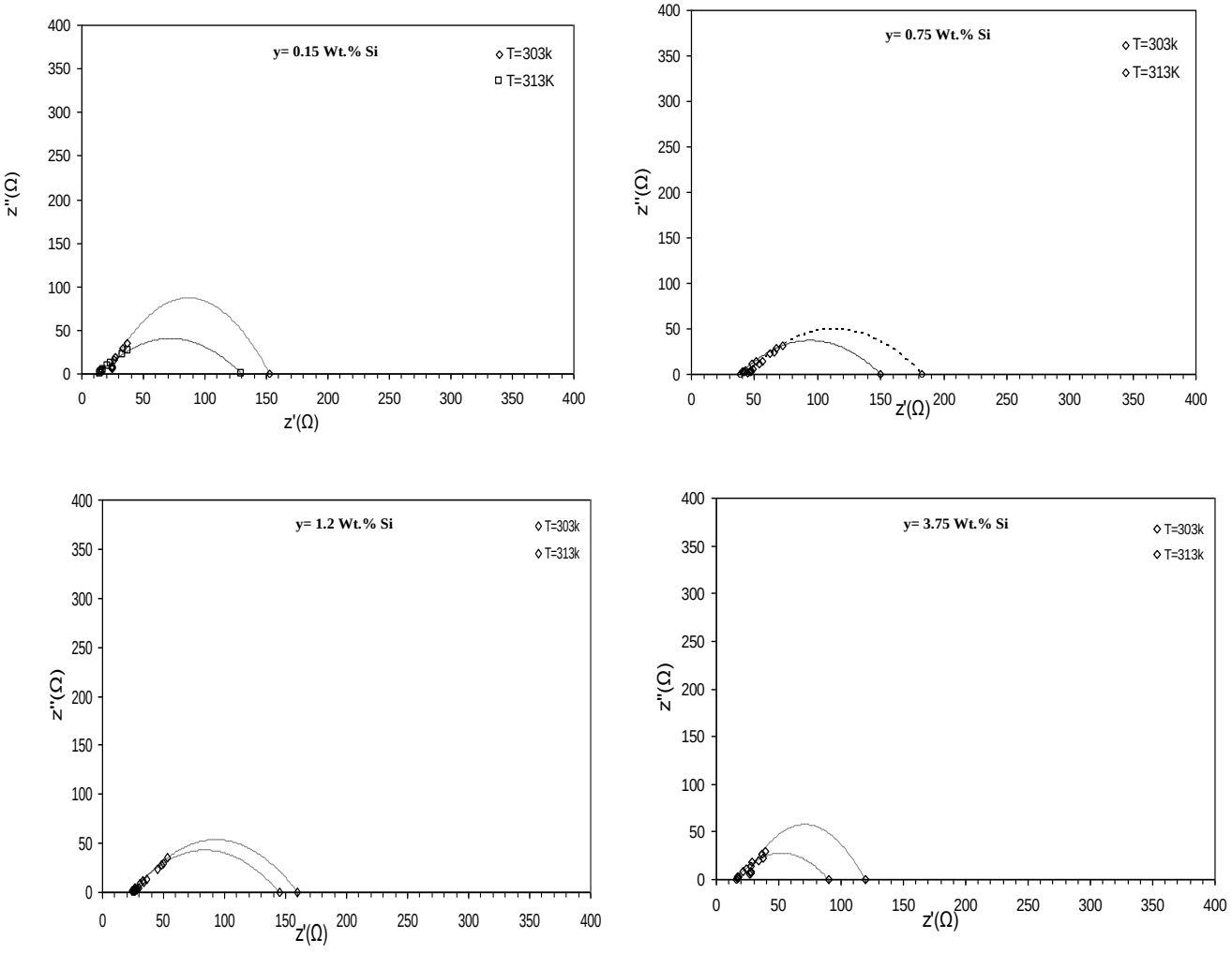

Fig.(4.14): Complex Cole–Cole plot of impedance for ((PVA: 0.5 $NaHSO_4$) : 9.9 wt.% EC/ y Si) with different Si concentration at T=303K, T=313K.

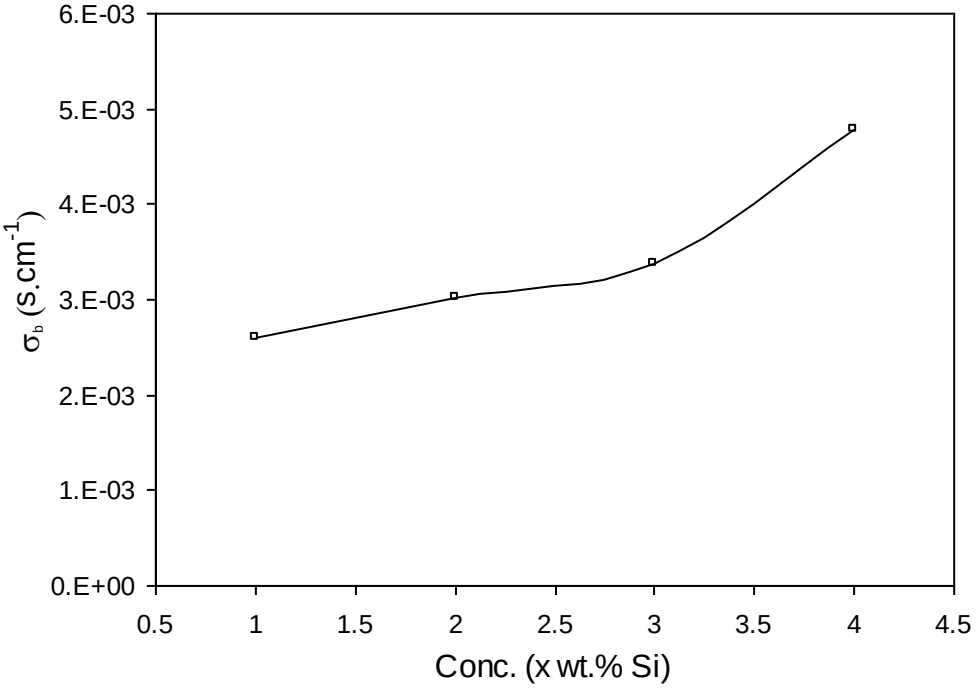

Fig.(4.15): Bulk conductivity of ((PVA: 0.5 $NaHSO_4$) : 9.9 wt. % EC/ y Si) versus Si concentration at room temperature.

4.6 AC Conductivity for Polymer Electrolyte

Fig.(4.16) shows the variation of ac conductivity as a function of inverse temperature for ((PVA: 0.5 $NaHSO_4$) / x EC) with x=(0, 3.3, 6.6, 9.9, 13.2, 16.5& 19.8 wt. %). The plot shows that as temperature increases, the conductivity increases. Regression values are close to (0.91-0.99) suggesting that all the points lie on a straight line. The conductivity values for the PSAPE do not show any abrupt jump with temperature indicating that these electrolytes exhibit a completely amorphous nature that facilitates the fast ion motion in the polymer net work and it further provides a higher free volume in the polymer electrolyte upon increase in temperature. The temperature dependence of conductivity can be described by [77],

$$\sigma_{ac}.T = \sigma_o \exp(\frac{-E_a}{KT}) \qquad (4.5)$$

where σ_o is the temperature independent constant , E_a is activation energy, K is Boltzman constant and T is absolute temperature. The activation energies for ion migration calculated from the slope of the log σT vs.10^3/T plots, are given in Table (4.7). It is clear, the E_a value for all samples ranges from 0.11 to 0.26 eV. It is noteworthy that the polymer electrolytes with low values of activation energies are desirable for practical applications.

The temperature dependence of conductivity for polymer electrolytes ((PVA: 0.5 $NaHSO_4$): 9.9 wt. % EC/ y Si) where (y=0.15, 0.75, 1.2 and 3.75 wt. %) is shown in Fig.(4.17). As there is no sudden change in the value of conductivity with temperature, it may be inferred that these electrolyte do not undergo any phase transitions within the temperature range investigated [6]. There is a significant conductivity

enhancement due to the addition of the plasticizer, EC to SAPE. Also, the presence of (Si) has shown a conductivity enhancement of the PSAPE. The highest room temperature conductivity enhancement was obtained for ((PVA: 0.5 $NaHSO_4$): 9.9 wt. % EC/ y Si) was 1×10^{-2} $S.cm^{-1}$ (at 303 K). The activation energies for ion migration calculated from the slope of the $\log \sigma T$ vs.10^3/T plots, are given in Table (4.8). It is clear, the E_a value for all samples ranges from 0.07 to 1.8eV.

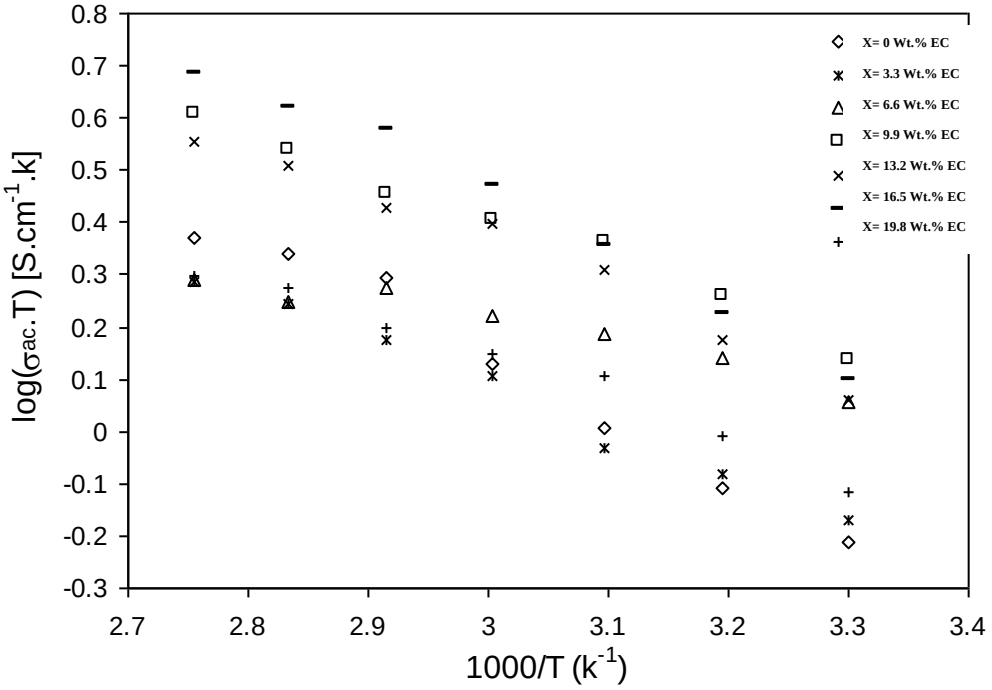

Fig.(4.16): Temperature dependence of the ac conductivity for ((PVA: 0.5 $NaHSO_4$) / x EC) with different EC concentrations.

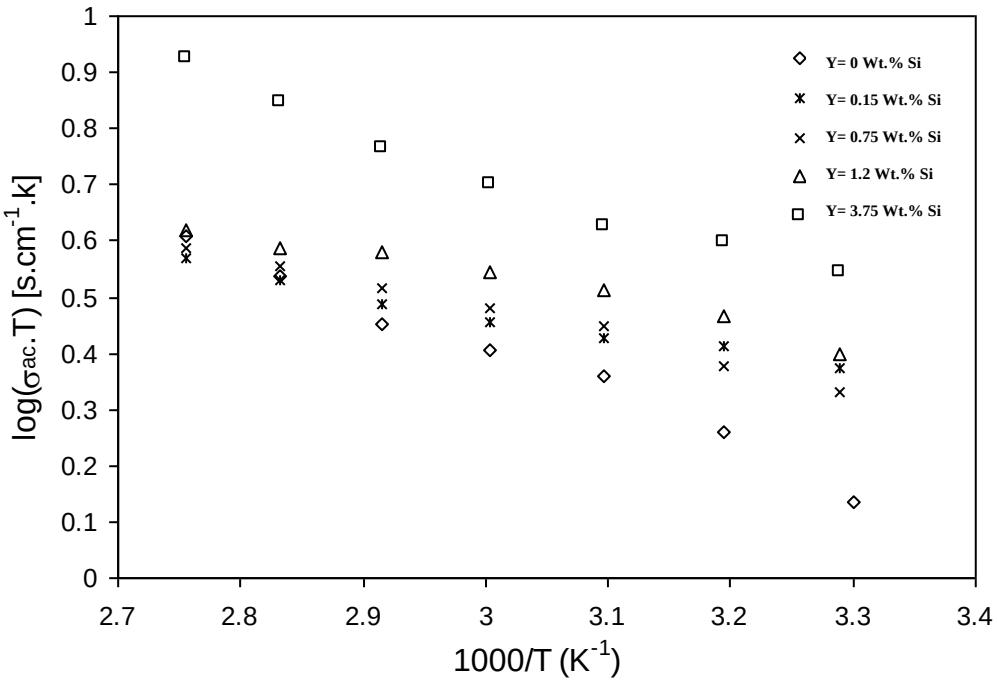

Fig.(4.17): Temperature dependence of the ac conductivity for ((PVA: 0.5 $NaHSO_4$) : 9.9 wt.% EC/ y Si) with different Si concentrations.

4.7 Frequency Dependent Conductivity for Polymer Electrolytes

Fig.(4.18) shows the variation of σ_{ac} with the frequency for ((PVA: 0.5 $NaHSO_4$) / x EC) with x= (0, 3.3, 6.6, 9.9, 13.2, 16.5& 19.8 wt.%). It can be observed that the conductivity increases gradually as frequency increases obeying the universal power law relation [15, 75].

$$\sigma_{ac} \alpha \omega^n \qquad (4.6)$$

where, ω is the angular frequency and *n* is the power law exponent. The value of *n* is obtained by least square fitting equation (4.6) where n_1 and n_2 , are tabulated in Table (4.7) from the table it is clear that the value of *n* vicinity between 0.06 and 0.2. This result are less than 0.2 which in the class of fast ionic conductor [15, 75].

Fig.(4.19) shows the variation of σ_{ac} with the frequency for ((PVA: 0.5 $NaHSO_4$) : 9.9 wt.% EC/ y Si) with y= (0.15, 0.75, 1.2 & 3.75 wt.%). It can be observed that the conductivity increases gradually as frequency increases obeying equation (4.6). The values of n_1 and n_2 are in Table (4.8). From the table it is clear that the value of *n* vicinity between 0.2 and 0.05. These results agree with fast ionic conductor.

Table (4.7): Effect of EC concentration on activation energies (E_a) and conduction index (n) values of ((PVA: 0.5 $NaHSO_4$) / x EC) with different EC concentration.

x wt.% (EC)	E_a(eV)	n_1	n_2
0	0.26	0.2	0.2
3.3	0.18	0.2	0.12
6.6	0.11	0.2	0.09
9.9	0.16	0.18	0.1
13.2	0.18	0.19	0.1
16.5	0.22	0.15	0.1
19.8	0.16	0.15	0.06

Table (4.8): Effect of Si concentration on activation energies (E_a) and conduction index (n) values of ((PVA: 0.5 $NaHSO_4$): 9.9 wt. % EC/ y Si)

x wt.% (Si)	E_a(eV)	n_1	n_2
0.15	0.07	0.17	0.05
0.75	0.092	0.2	0.1
1.2	0.094	0.16	0.06
3.75	0.18	0.2	0.08

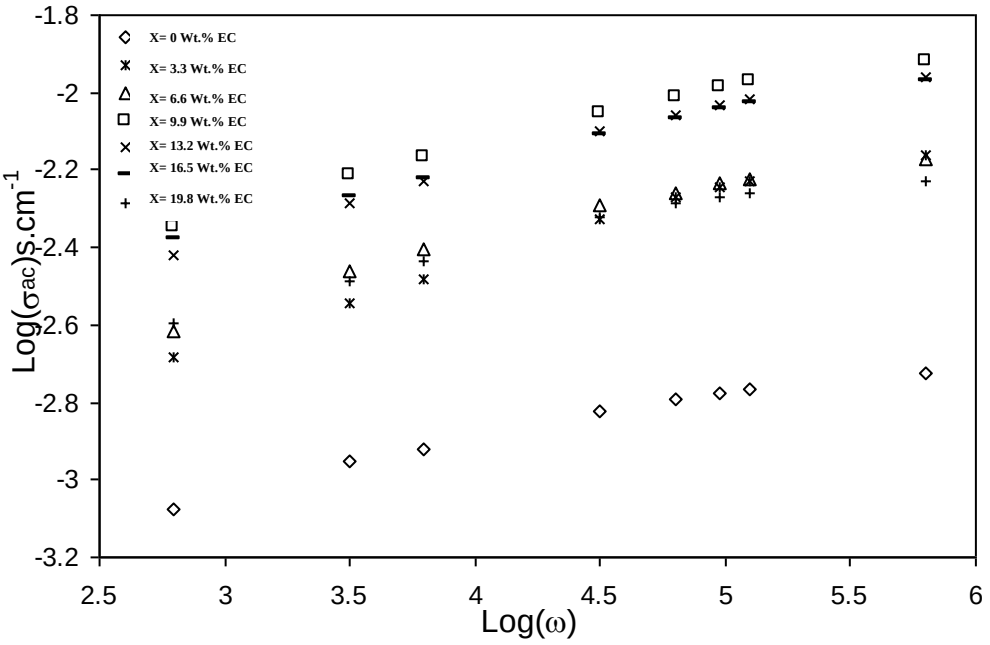

Fig.(4.18): Variation of the ac conductivity $\sigma_{ac}(\omega)$ with frequency for ((PVA: 0.5 $NaHSO_4$) / x EC) with different EC concentrations at room temperature.

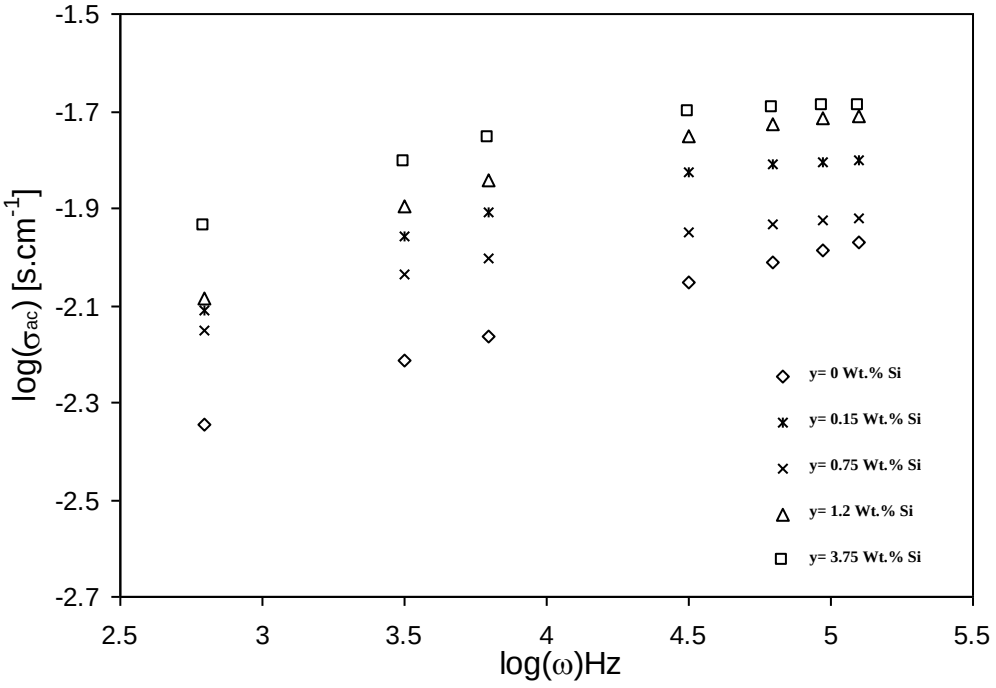

Fig.(4.19): Variation of the ac conductivity $\sigma_{ac}(\omega)$ with frequency for ((PVA: 0.5 $NaHSO_4$) : 9.9 wt.% EC/ y Si) with different Si concentrations at room temperature

4.8 Frequency Dependence of the Dielectric Parameters

Fig.(4.20) show the variation of the dielectric constant ε' versus frequency at room temperature 303 K. It can be noticed that ε' decreases monotonically with increasing frequency in the frequency range of $\omega\tau >> 1$ for all polymer electrolyte. This behavior can be described by the Debye dispersion relations [80],

$$\varepsilon' \cong \varepsilon_{\infty} + \frac{\varepsilon_s - \varepsilon_{\infty}}{1 + \omega^2 \tau^2} \qquad (4.7)$$

The variation of dielectric constant ε' as a function of frequency for all polymer electrolytes at room temperture (Fig.(4.20)) indicates that at low frequencies the dielectric constant is high due to the intervatial polarization. There is a decrease in dielectric constant towards higher frequencies due to the high periodic reversal of the applied field.

Fig.(4.21) show the variation of the dielectric constant ε' versus EC concentration at room temperature. The dielectric constant ε' has been experimentally found to increase with increase EC concentration upto 9.9 wt.% EC and then its decreases with increasing EC concentration. The increase in the value of dielectric constant indicates that there is an increase in charge carrier concentration and hence the increase in conductivity [82], the decrease in dielectric constant for further addition of EC concentration leads to the formation of ion aggregation, which causes a fall in mobility of charge carriers and cause a significant fall in ionic conductivity in accordance with Fig.(4.12). The higher value of ε' for polymer electrolyte (9.9 wt. % EC) is due to the enhanced charge density at the space charge accumulation region.

Fig.(4.22) shows the variation of ε′ with frequency for ((PVA: 0.5 $NaHSO_4$) : 9.9 wt.% EC/ y Si) with y= 0.15, 0.75, 1.2and 3.75 wt.% at room temperature. It can be noticed that ε' decreases monotonically with increasing frequency in the frequency range of $\omega\tau >> 1$ for all polymer electrolyte. This behavior can be described by the Debye dispersion The high dielectric permittivity obtained in the present study could be attributed to the delocalization of charge carriers. The higher value of ε′ for polymer electrolyte at y=3.75 is due to the enhanced charge density at the space charge accumulation region.

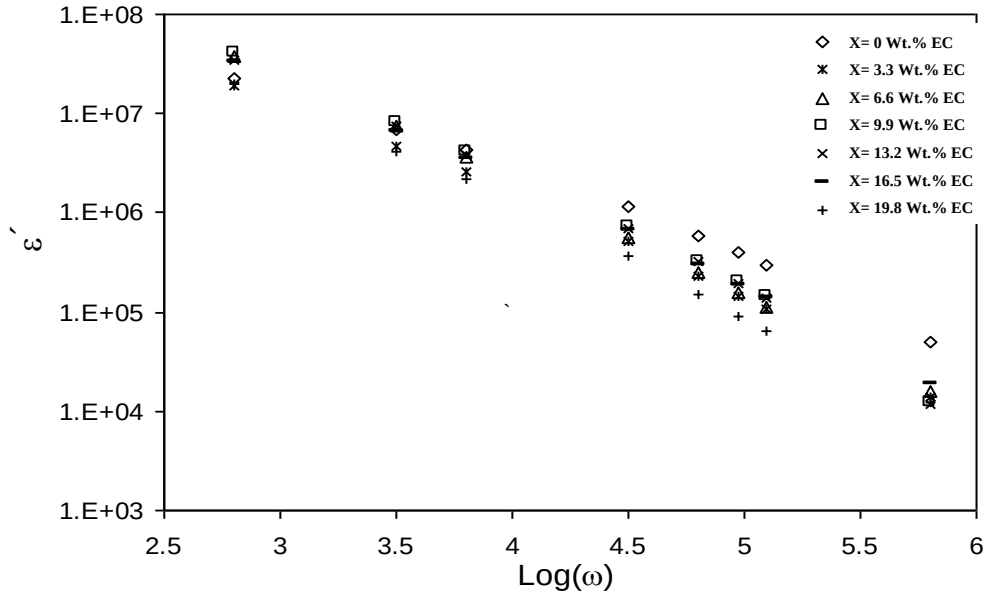

Fig.(4.20): Variation of dielectric constant ε′ as function of frequency for ((PVA: 0.5 $NaHSO_4$) :/ x EC) with different EC concentrations at room temperature.

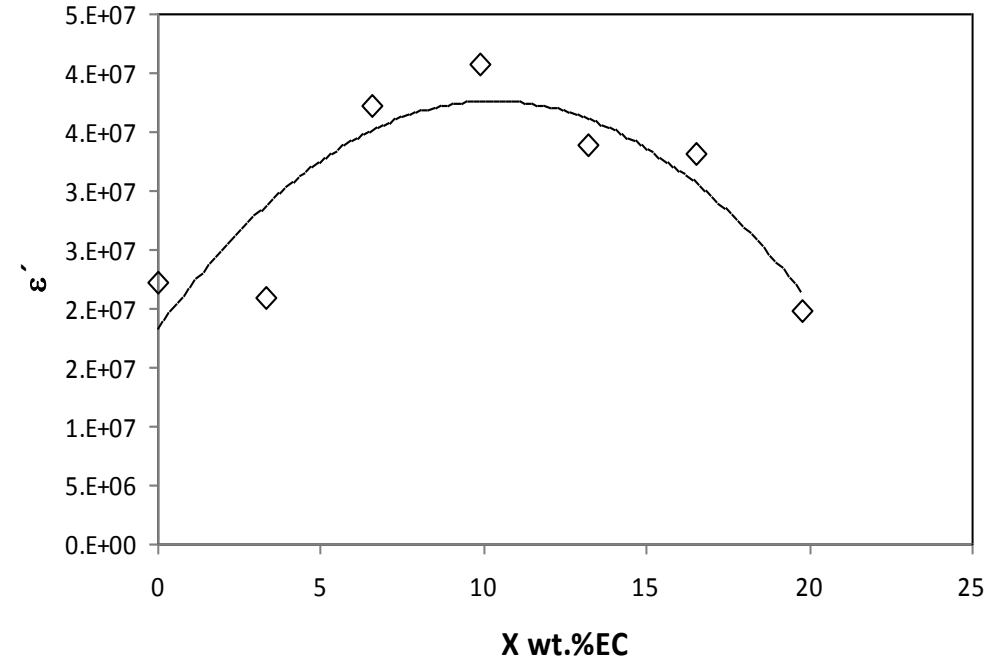

Fig.(4.21): Variation of dielectric constant ε′ versus EC concentration for ((PVA: 0.5 $NaHSO_4$) / x EC) at room temperature & 100 HZ.

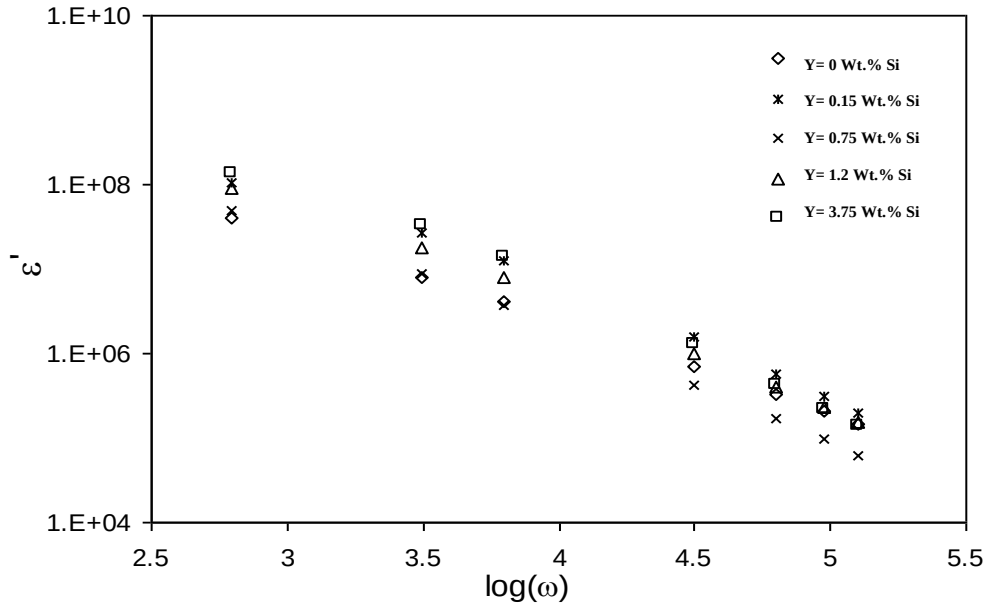

Fig.(4.22): Variation of dielectric constant ε′ as function of frequency for ((PVA: 0.5 $NaHSO_4$) : 9.9 wt.% EC/ y Si) with different Si concentrations at room temperature.

4.9 Temperature Dependence of the Dielectric Parameters

Dielectric constant (ε′) is representative of stored charge in a material. Fig.(4.23) and (4.24) show the variation of dielectric constant as a function of temperature for ((PVA: 0.5 $NaHSO_4$) / x EC) with different EC concentrations and **(**(PVA: 0.5 $NaHSO_4$) : 9.9 wt.% EC/ y Si) with different Si concentrations at 100 Hz respectively. It is clear that ε' increases with increase temperature. The variation of ε' with temperature is different for non-polar and polar polymers. In general, non-polar polymers ε' is independent of temperature, but in the case of polar polymers the ε' increases with the increase of temperature. This behavior is typical of polar dielectrics, in which the orientation of dipoles is facilitated with rising temperature and thereby the permittivity is increased [76]. The dielectric constant increases with temperature because the orientation is facilitated as the temperature increases. The increasing value of ε' with increasing temperature is mainly due to the migration polarization of the mobile ions, where the drop in the viscosity of the medium facilitates the orientation of dipoles.

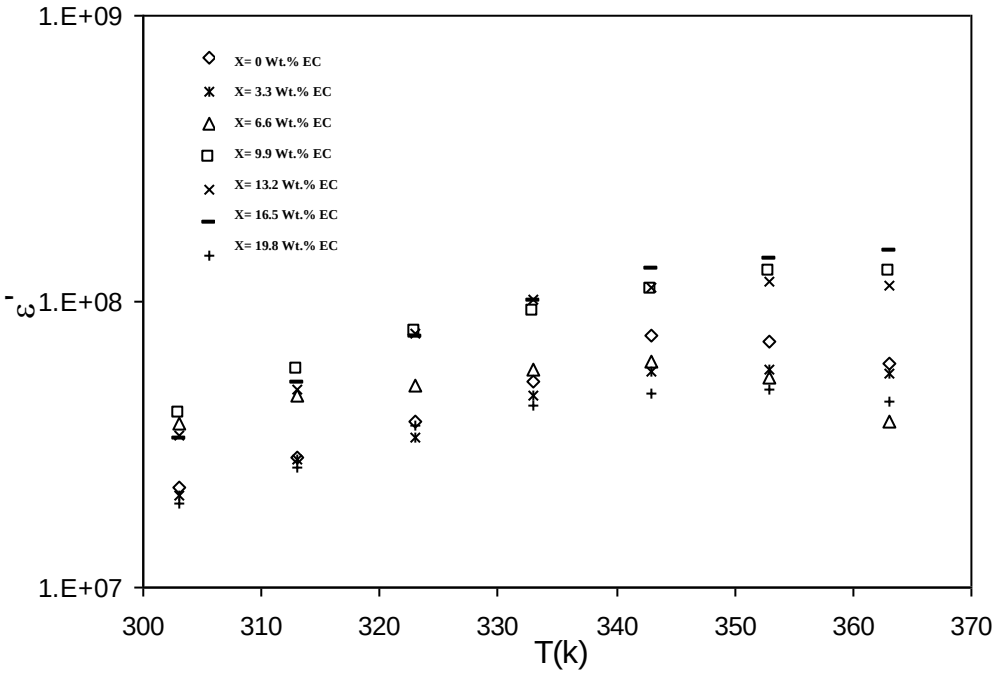

Fig.(4.23): Variation of dielectric constant ε′ as function of temperature for ((PVA: 0.5 $NaHSO_4$) / x EC) with different EC concentrations at 100 HZ.

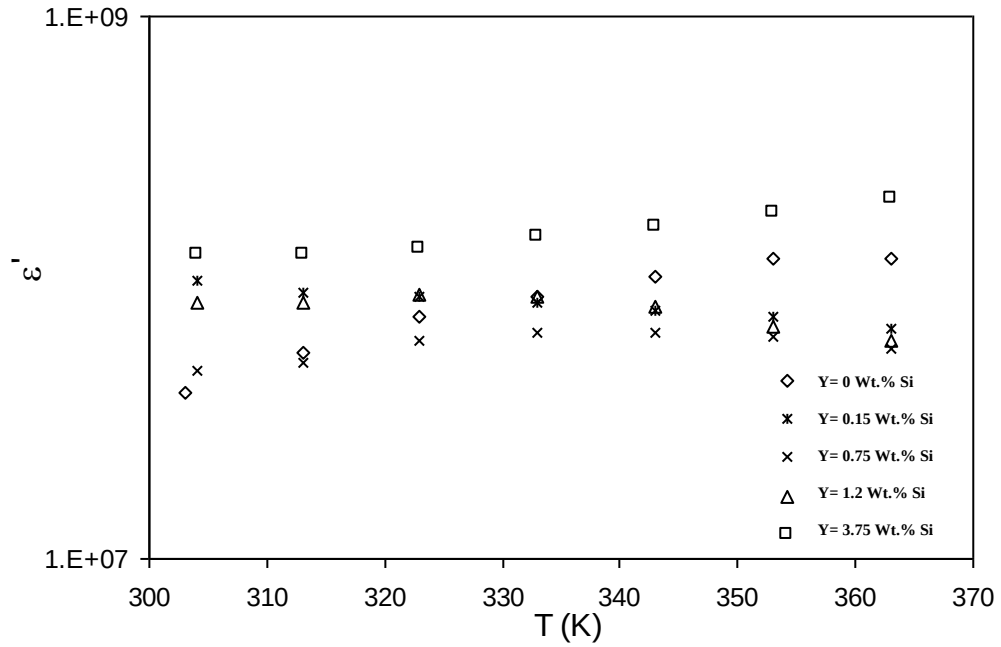

Fig.(4.24): Variation of dielectric constant ε′ as function of temperature for ((PVA: 0.5 $NaHSO_4$) : 9.9 wt.% EC/ y Si) with different Si concentrations at 100 HZ.

4.10 Transference Number Measurement

Transference number is an important parameter in studying type of conduction in solid polymer electrolyte. The transference numbers, both ionic (t_{ion}) and electronic (t_{ele}), of the electrolyte were evaluated using the Wagner's polarization techniques. The dc current was monitored as a function of time on application of fixed dc voltages 1.5volt across Cu / ((PVA: 0.5 $NaHSO_4$) / x EC)/Cu. Fig.(4.25) illustrates current versus time plot for the electrolyte with different EC concentration (x=0, 6.6 , 9.9 , 13.2 and 19.8 wt.%). The initial current is due to the total current (i_t) which is due to the ionic (i_{ion}) and the electronic (i_{ele}). As the polarization build up the i_{ion} is blocked and the final current is only the electronic current [77, 78].

$$i_\tau = i_{ele} + i_{ion}$$

And

$$t_{ion} = \frac{i_\tau - i_{ele}}{i_\tau}$$

$$t_{ele} = \frac{i_{ele}}{i_\tau}$$

The transference number has been extracted and given in Table (4.9). Fig.(4.26) shows current versus time plot for the electrolyte ((PVA: 0.5 $NaHSO_4$) : 9.9 wt.% EC/ y Si) where y= 0.15, 0.75, 1.2, and 3.75 wt.%. The estimated values of the ionic transparent number are given in Table (4.10). Since the electron fraction is t_{ele}=0.01 and ion fraction is t_{ion}=0.99 for all samples except the blank sample the electron fraction is (t_{ele})=0.03 and ion fraction is (t_{ion})=0.97 so, current is predominantly due to ions with negligible contribution coming from the electrons.

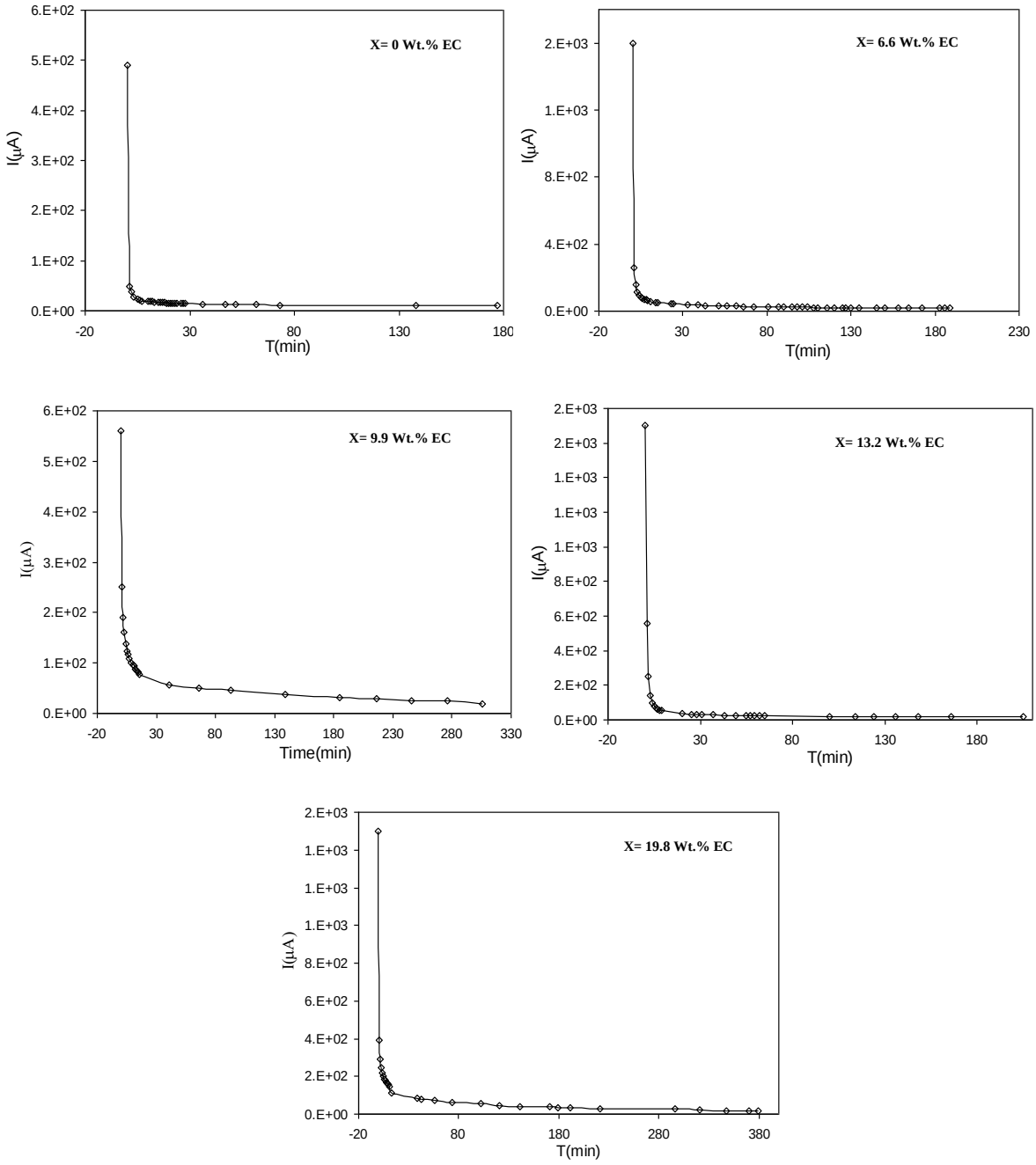

Fig.(4.25): Polarization current as a function of time for ((PVA: 0.5 $NaHSO_4$) / x EC) electrolyte with different EC concentration at room temperature.

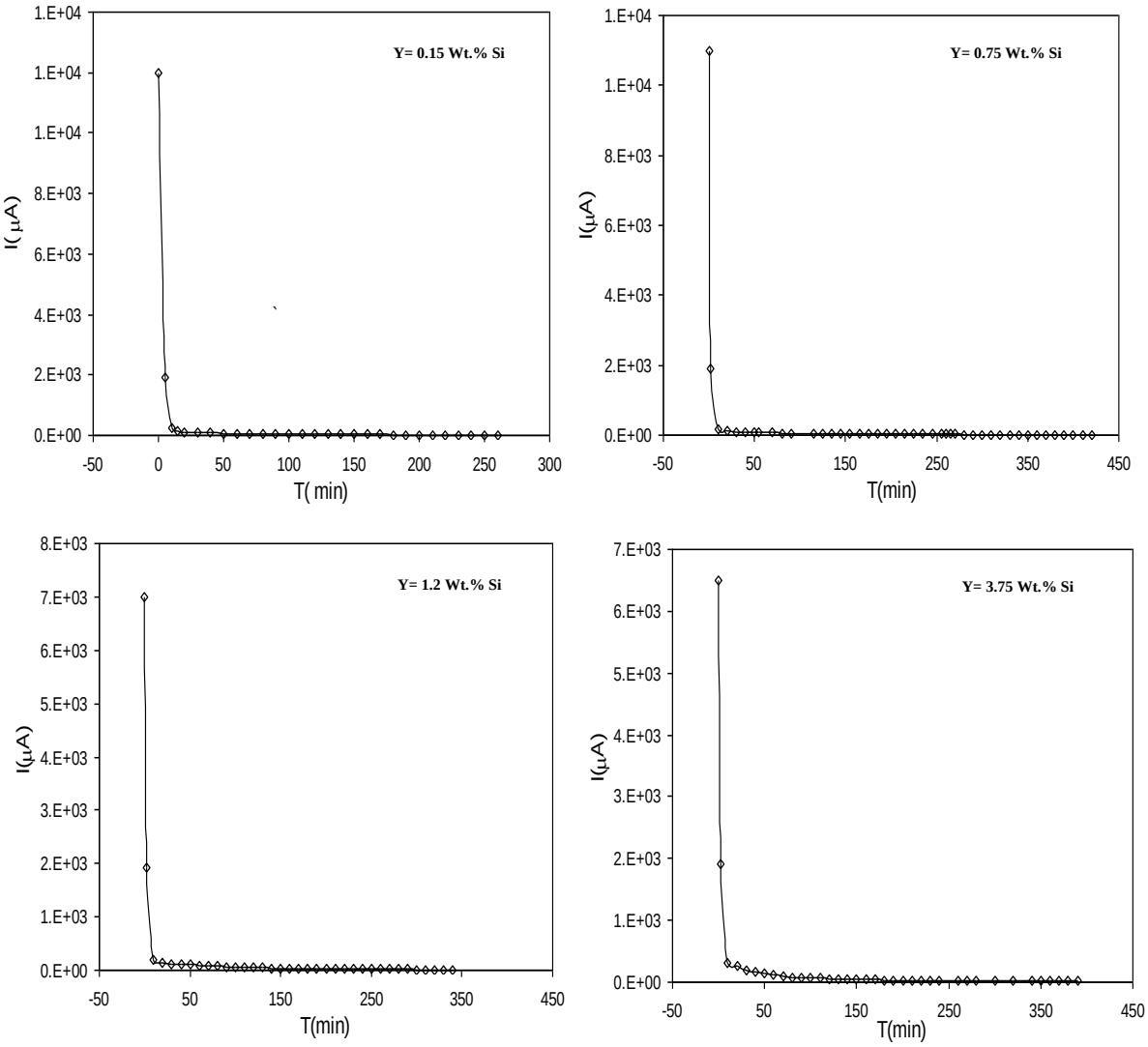

Fig.(4.26): Polarization current as a function of time for ((PVA: 0.5 $NaHSO_4$) : 9.9 wt.% EC/ y Si) electrolyte with different Si concentration at room temperature.

Table (4.9): Effect of EC concentration on ionic transport number for ((PVA: 0.5 $NaHSO_4$) / x EC) polymer electrolyte.

x **wt. % (EC)**	**Ion fraction**
0	**0.97**
6.6	**0.99**
9.9	**0.99**
13.2	**0.99**
19.8	**0.99**

Table (4.10): Effect of Si concentration on ionic transport number for ((PVA: 0.5 $NaHSO_4$): 9.9 wt. % EC/ y Si) polymer electrolyte.

x **wt.% (Si)**	**Ion fraction**
0.15	**0.99**
0.75	**0.99**
1.2	**0.99**
3.75	**0.99**

4.11 Discharge characteristic of the cell

Open circuit voltage (OCV) of the cell was measured by storing it in an open-circuit condition for 24h at room temperature. Fig.(4.27a) shows OCV of the Mg /((PVA: 0.5 $NaHSO_4$) : 9.9 wt.% EC)/MnO_2 cell at room temperature. It is clear that the OCV was constant at 2.4±0.05 *V* for 24 hour of storage.

Fig.(4.27b) shows the discharge characteristic of the cell Mg/((PVA: 0.5 $NaHSO_4$) : 9.9 wt.% EC)/MnO_2 at constant load, R=50 kΩ. The discharge voltage was sustained for 45h until the cut-off voltage of 1.91*V*. The value of the discharge capacity C was evaluated from the following equation [81, 82].

$$C = \frac{1}{R}\int_0^t V(t)dt \qquad (4.8)$$

by integrating the area under the curve of Fig.(4.27b). The discharge capacity estimated by 2.49 mAh actually, estimated capacitance is only for surface area of electrode. Since the electrodes used in this cell is in compact planar form, this mean that electrodes are not fully utilized for discharge reaction. The active weight of Mg was deduced by < 0.01 gm. Therefore, the real discharge capacity can be estimated by >249mAh/gm for Mg / Mno_2. After Mg / Mno_2 were fully discharged, a layer of white powder was formed. The *XRD* confirmed that the white powder is $MgSO_4$. Based on the *XRD* data, the failure of the anode is due to the sulfation of Mg which formed $MgSO_4$. Sulfation [83] is the number one cause of the battery failure. It is identified empirically by observing the effects of: Loss of capacity, Loss of voltage and increase in internal resistance.

Fig.(4.28) shows the discharge characteristic of the battery Mg / ((PVA: 0.5 $NaHSO_4$) : 9.9 wt.% EC: y wt.% Si) / FeS_2 at constant load, R=50 kΩ. The discharge voltage was sustained for 67.5h until the cut-off voltage of 0.51*V*. The extracted value of cell capacity for Mg /((PVA: 0.5 $NaHSO_4$) : 9.9 wt.% EC: y wt.% Si)/ FeS_2 was 1.12 mAh which evaluated from equation (4.8) by integrating the area under the curve (4.28). The active weight of Mg was deduced by < 0.01 gm. Therefore, the real discharge capacity can be estimated by >112 mAh/gm.

Fig. (4.29) shows the *I-V* and *J-P* characteristics for Mg / ((PVA: 0.5 $NaHSO_4$): 9.9wt. % EC) /MnO_2 battery at room temperature. The *I-V* curve had a simple linear form which indicates that polarization on the electrode was primarily dominated by ohmic contributions. The internal resistance of the Mg / MnO_2 battery was obtained from the gradient of the *I-V* graph, which was 165Ω. The voltage of the Mg / Mno_2 battery dropped to a short circuit density of 1.61mA/cm^2 and maximum power density 3.45mW/cm^2

Fig.(4.30) shows the *I-V* and *J-P* characteristics for Mg /((PVA: 0.5 $NaHSO_4$) : 9.9wt. % EC: 3.75wt. % Si) / FeS_2 battery at room temperature. *I-V* curve had a simple linear form which indicates that polarization on the electrode was primarily dominated by ohmic contributions. The internal resistance of the Mg / FeS_2 battery was obtained from the gradient of the *I-V* graph, which was 160Ω. The voltage of the Mg / FeS_2 battery dropped to a short circuit density of 1.3mA/cm^2 and maximum power density 2.2 mW/cm^2.

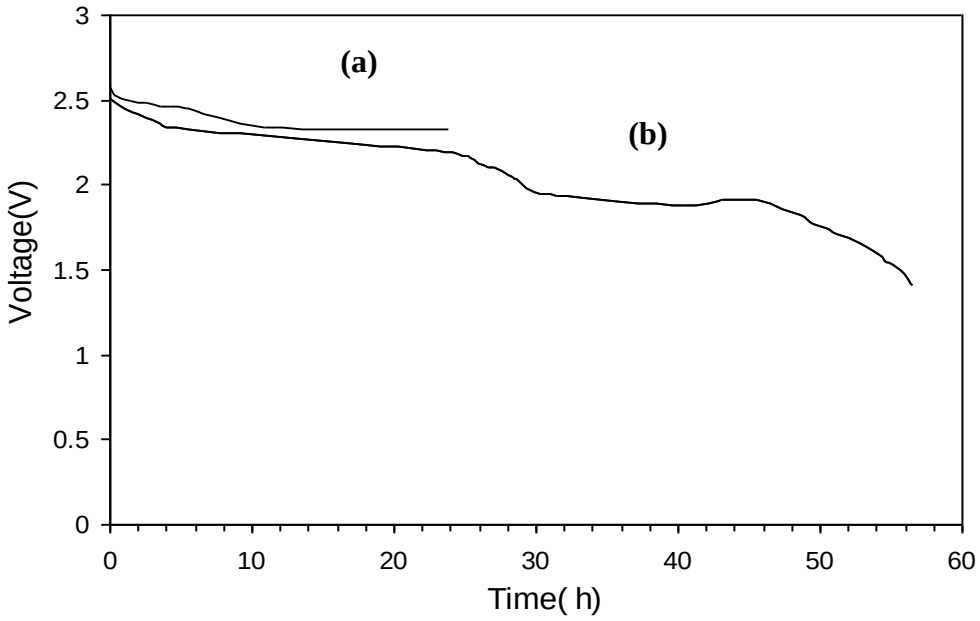

Fig.(4.27): (a) OCV for Mg/((PVA: 0.5 $NaHSO_4$) : 9.9 wt.% EC)/MnO_2 cell during 24h of storage, (b) Discharge plot for Mg/((PVA: 0.5 $NaHSO_4$) : 9.9wt.% EC)/MnO_2 cell at constant load of 50 kΩ.

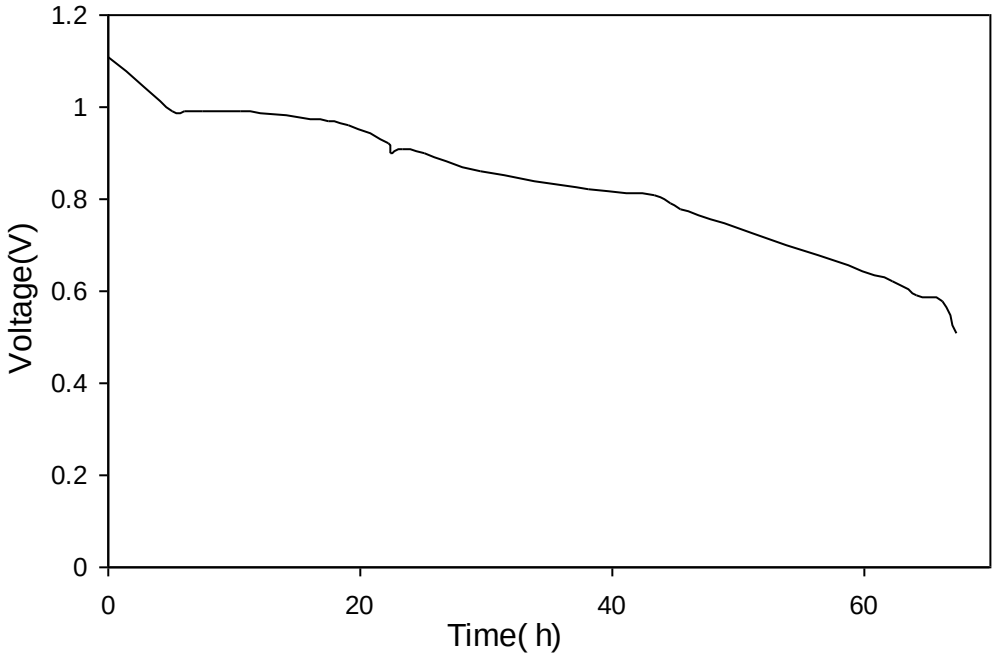

Fig.(4.28): Discharge plot for Mg/((PVA: 0.5 $NaHSO_4$) : 9.9 wt.% EC: 3.75 wt.% Si)/ FeS_2 cell at constant load of 50 kΩ.

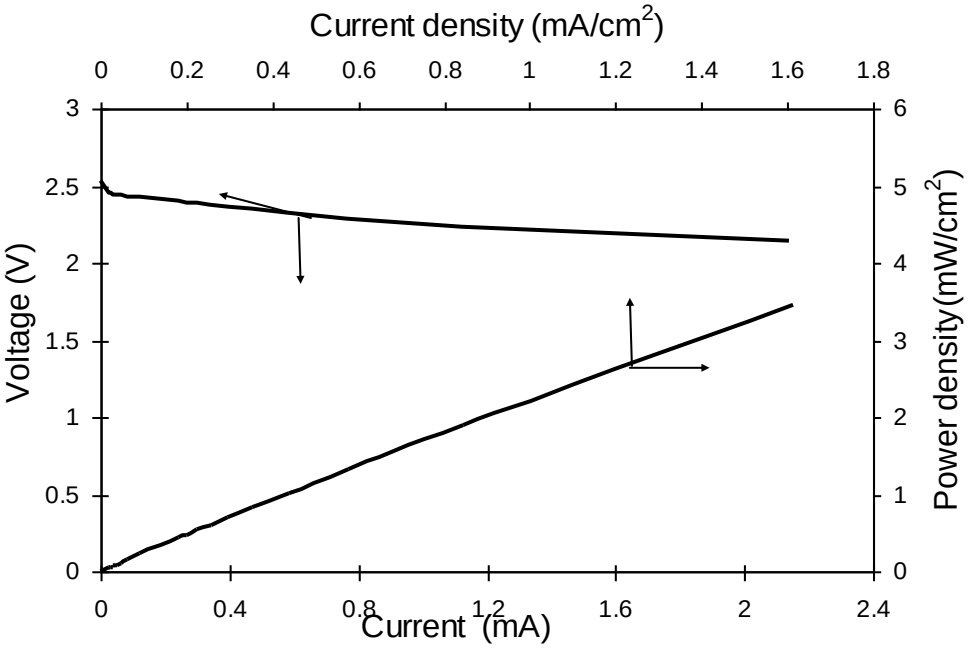

Fig.(4.29): I-V and J-P curves for Mg/((PVA: 0.5 $NaHSO_4$) : 9.9 wt.% EC)/MnO_2 cell.

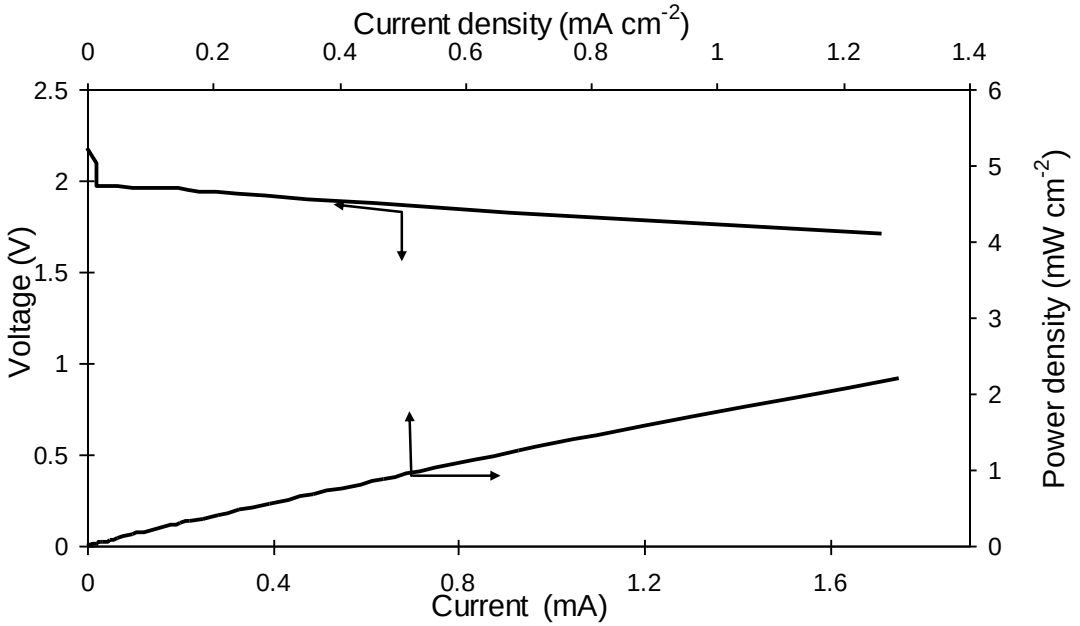

Fig.(4.30): I-V and J-P curves for Mg/((PVA: 0.5 $NaHSO_4$) : 9.9 wt.% EC: 3.75 wt.% Si)/FeS_2 cell.

4.12 Electrode Characteristic

Solid electrolyte battery has been constructed using Mg as anode and Mno_2 as cathode according to the configuration Mg/ ((PVA: 0.5 $NaHSO_4$): 9.9 wt. % EC)/MnO_2, shown in Fig.(3.1a). In the present study the effect of the chemical reaction of the electrode material with the electrolyte has been taken in consideration. XRD of both anode Mg and cathode MnO_2 were performed after discharged the cell. Fig.(4.31 a & b) illustrate the comparative XRD patterns of the virgin Mg anode and after discharge. The XRD pattern indicated that some of characteristic peaks disappeared where as new peak appeared, the observed peaks matched quite well with *JCPDS* file No. 72-1068 for $MgSO_4$ at 2θ= 16.25, 17.37, 18.7, 20.2, 22.01, 30.8 and 33.34. Thus, it is confirmed that the new structure is indeed $MgSO_4$.

Fig. (4.32 a & b) shows the comparative *XRD* patterns of virgin MnO_2 cathode and after the discharge. After discharge, *XRD* pattern indicated that some of characteristic peaks disappeared where new peak appeared, the observed peaks matched quite well with *JCPDS* file No.74-1842 for MnOOH at 2θ= 26.38 and 35.65. Thus, it is confirmed that the structure is indeed MnOOH. Therefore, the expected chemical reaction that probably takes place in the cell,

At the anode: $\frac{1}{2}Mg + \frac{1}{2} SO_4^{-2} \rightarrow \frac{1}{2} (MgSO_4) + e^-$

At the cathode: $MnO_2 + H^+ + e^- \rightarrow MnOOH$

Overall reaction:

$$\frac{1}{2}Mg + MnO_2 + H^+ + \frac{1}{2}SO_4^{-2} \rightarrow MnOOH + \frac{1}{2} (MgSO_4)$$

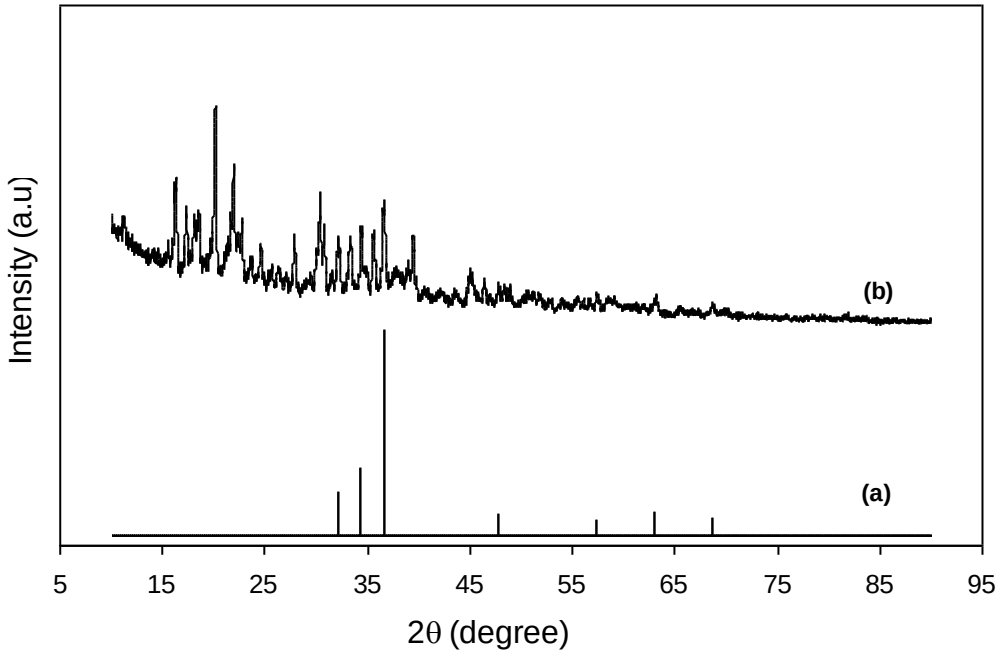

Fig.(4.31): XRD patterns of Mg electrode (a) Virgin Mg, (b) Mg after complete discharge at 50 kΩ.

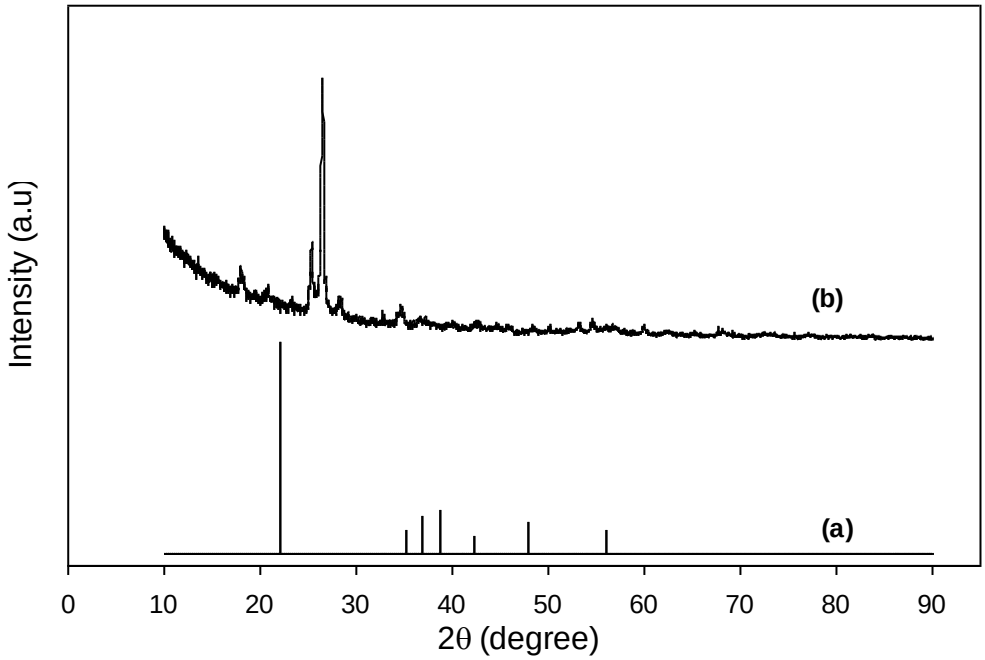

Fig.(4.32): XRD patterns of MnO_2 electrode (a) Virgin MnO_2, (b) MnO_2 after complete discharge at 50 kΩ.

The study was extended to the other electrolyte containing Si which has higher conductivity using Mg as anode and FeS_2 as cathode shown in Fig.(3.1b). Fig.(4.33 a & b) shows the comparative *XRD* patterns of virgin Mg and Mg after discharge. The *XRD* pattern indicated that some characterist peak disappeared where as new peak appeared after discharge, the observed peaks matched quite well with *JCPDS* file No. 72-1068 for $MgSO_4$ at 2θ= 15, 34.6 and 36.9. Thus, it is confirmed that the structure is indeed $MgSO_4$.

Fig.(4.34 a & b) shows the comparative *XRD* patterns of the vergin FeS_2 cathode and after the discharge, respectively. After discharge the *XRD* pattern indicated that FeS_2 deosnot change, the characterist peak also not change but intensity of the peak decrease. The drop in the intensity of the peak can be attribute to the strain experine due to the interculation of the ion with FeS_2 during discharge.

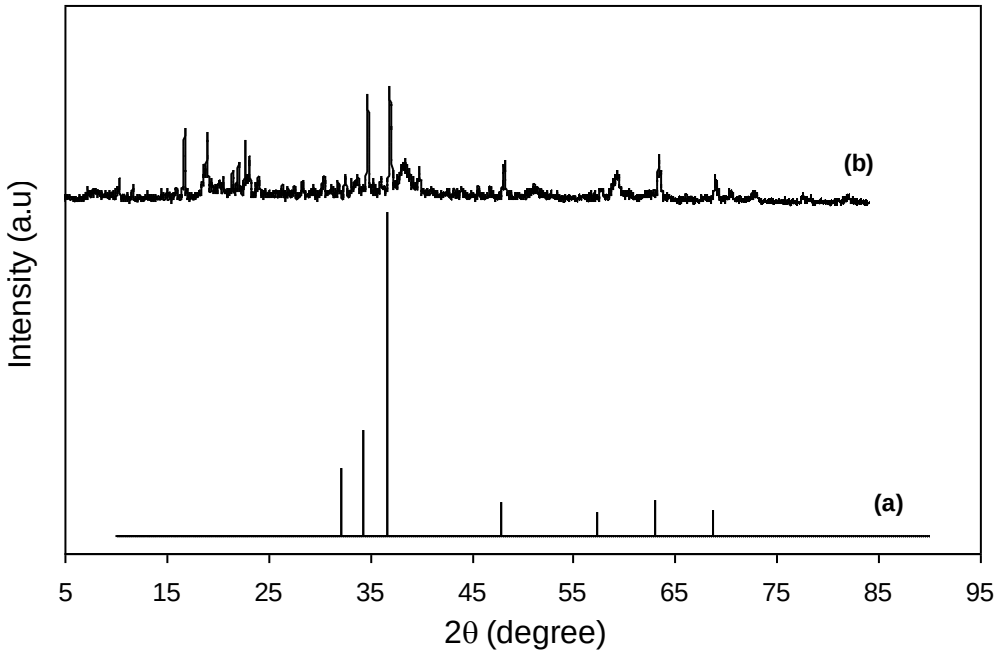

Fig.(4.33): XRD patterns of Mg electrode (a) Virgin Mg, (b) Mg after complete discharge at 50 kΩ.

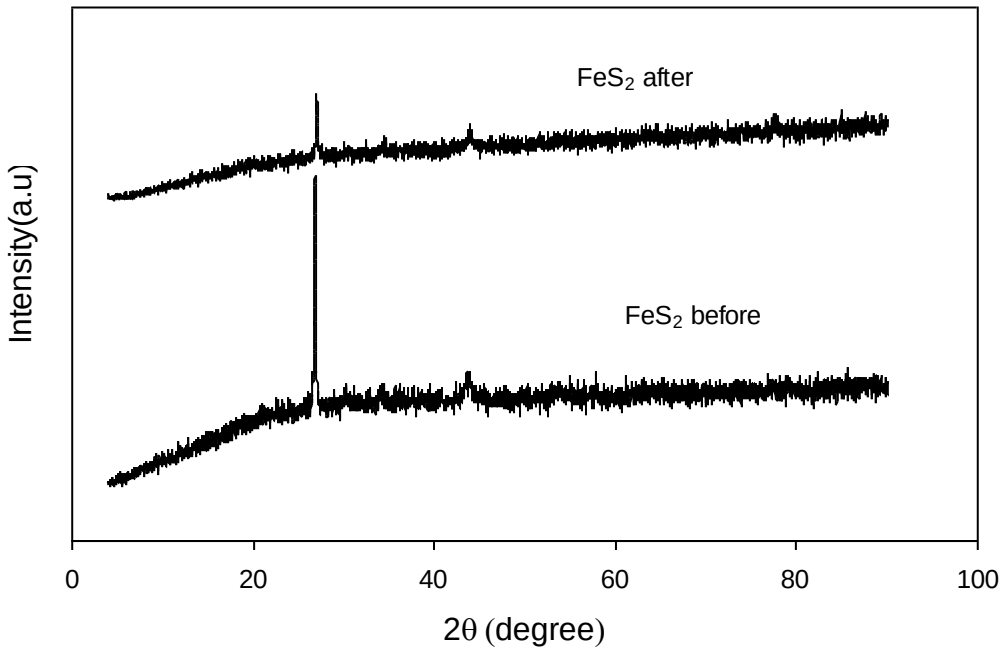

Fig.(4.34): XRD patterns of FeS_2 electrode (a) Virgin FeS_2, (b) FeS_2 after complete discharge at 50 kΩ.